THE UNIVERSITY OF OKLAHOMA
GRADUATE COLLEGE

A PALEOMAGNETIC AND DIAGENETIC STUDY OF THE KENTLAND IMPACT CRATER

A THESIS
SUBMITTED TO THE GRADUATE FACULTY
in partial fulfillment of the requirements for the
Degree of
MASTER OF SCIENCE

By

CHRISTINA HAMILTON
Norman, Oklahoma
2019

Downloaded from SHAREOK. Persistent Handle URL: https://hdl.handle.net/11244/319636

A PALEOMAGNETIC AND DIAGENETIC STUDY OF THE KENTLAND IMPACT CRATER

A THESIS APPROVED FOR THE
CONOCOPHILLIPS SCHOOL OF GEOLOGY AND GEOPHYSICS

BY

Dr. Richard Douglas Elmore, Chair

Dr. Shannon Dulin

Dr. Michael Soreghan

© Copyright by CHRISTINA HAMILTON 2019
All Rights Reserved.

Acknowledgements

Firstly, I would like to thank my advisor Dr. R. Douglas Elmore. Thank you for bestowing this interesting geologic story upon me and thank you for letting me strengthen my love for the subject of Geology. Thank you for putting up with my many emotions throughout this journey and thank you for your patience and guidance. I could not ask for a better professor and mentor.

Thank you to my committee members Dr. Shannon Dulin and Dr. Michael Soreghan for taking the time to read my thesis and provide me with both corrections and guidance during this journey. Your feedback is invaluable. I would also like to extend my utmost gratitude for Dr. Dulin, who graciously went out to the field with me to gather more data when Dr. Elmore was not able to do so.

I would also like to extend my thanks to Dr. John Weber who helped us gain access to the quarry and provided assistance in the field to collect the data in the quarry. He provided us with beautiful exposures that contained the polymict breccia dikes, which would have been difficult to find on our own. I would also like to extend my thanks to Dr. Weber's undergraduate students who also came out to the field to help with data collection.

Thank you to the quarry operator, Rich Miller, for allowing us to have access to the quarry to drill the samples that we needed. His inquisitive nature with respect to the timing of the impact and his geologic knowledge of the area was welcomed and I hope the results revealed from this study please him.

I am very thankful to my fellow graduate students, Gerhard Heij, Jeffrey Hardwick, Matthew Hamilton, and Kathryn Garrett for providing me with their expertise and providing helpful tips to better my research. Thank you for asking tough questions to help me gain a better understanding of my study and for aiding me in the use of some of the equipment used. I would

also like the thank the undergraduates who worked tirelessly to help me gather data, in particular Samantha Johnston.

I would like to thank my family, especially my parents, Scott and Lisa Hamilton for always providing me with the means to succeed. I will always be grateful for the sacrifices that you have made to get me where I am today. I would also like to thank my Aunty Selma for providing me with the encouragement and support when the work got tough. Her weekly skype sessions were appreciated and will be missed. Although she did not get to see me finish this chapter in life, I know she would be proud.

Last but not least, I would like to thank my fiancé Tanner Shadoan. Thank you for loving this bundle of stress. This thesis would not be complete without your pep talks and support.

Abstract

A paleomagnetic and petrographic study of host carbonate rocks and impact breccias at the Kentland impact structure was conducted to better constrain the timing of the impact and to better understand the and diagenetic evolution of the rocks. Stratigraphic constraints can only constrain the impact to between 325 Ma and 50 ka, although a previous paleomagnetic study of the host carbonate suggested a tentative Late Cretaceous age.

Ordovician-Silurian target carbonates dominate and are largely wackestone/packstone with minor dolomite and abundant allochems. Polymict impact breccias occur as dikes and consist of dolomite crystals with some clasts of the host carbonate, as well as, sandstone, sphalerite, apatite, and rare coated grains which contain clays, dolomite, calcite and hexagonal silica resembling tridymite. The host carbonates contain brecciated zones near the polymict breccias that display suevite-flow textures of aligned minerals including apatite and gypsum which occur as authigenic elongated crystals. Iron oxides, such as magnetite, hematite and potential goethite are also found within brecciated veins.

Vuggy porosity is present in the breccias and is attributed to escaping CO_2 that formed by sudden impact-related devolatilization. Porosity also occurs as partially to completely dissolved dolomite crystals as well as dissolved cement in sandstone clasts. These results suggest alteration by hydrothermal fluids, probably relatively soon after impact. Some breccias also show evidence of secondary hematite precipitation that occurs as cement and as replaced gypsum rosettes.

Alternating field and thermal demagnetization of impact breccia specimens removed two antipodal ancient components; one with southerly declinations and moderate negative inclinations and the other with northerly declinations and positive inclinations. Demagnetization of the host carbonates also removed these components. Isothermal remanent magnetization (IRM)

acquisition, coercivity modelling of the IRM, and thermal decay of the IRM show both low and high coercivity materials are present which indicate that the magnetization resides in magnetite and hematite. The demagnetization results and rock magnetic studies suggest the magnetization resides in magnetite at intermediate unblocking temperatures, whereas at higher temperatures it resides in hematite. These are interpreted as chemical remanent magnetizations (CRMs) that formed from alteration by hydrothermal fluids. The paleomagnetic pole falls on the Late Triassic to Early Jurassic part of the apparent polar wander path which suggests the alteration in the breccias, and probably the impact, occurred in the Late Triassic to Early Jurassic.

Table of Contents

Acknowledgements ..... **iv**

Abstract ..... **vi**

Table of Contents ..... **viii**

List of Figures ..... **x**

Introduction **1**

Geologic and Tectonic Background **5**

Methods **12**

Results and Interpretations **15**

Paleomagnetism 15

Specimens with Two Components *15*

Specimens with Southerly and Up Component *18*

Specimens with Northerly and Down Component *19*

Analysis of Specimen Directions *21*

Rock Magnetism 24

IRM Acquisition *24*

Triaxial Thermal Decay *26*

Diagenesis 28

Diagenesis of the Host Carbonates *28*

Diagenesis of the Transition Zones *29*

Diagenesis of the Polymict Breccias *32*

Discussion **36**

Origin and Timing of the Magnetization 36

Diagenesis of the Impact Crater.....39

Conclusion.....44

References.....46

List of Figures

Figure 1: The Kentland impact structure, highlighted in the red box, is located at 40°45'N and 87°24'W in Newton County, Indiana (Modified after Gray, 1989). It is a small complex crater that is ~6Km in diameter. The inset shows the approximate size of the crater (Modified after United States Meteorite Impact Craters, 2017). 4

Figure 2: Shatter cones that have formed within the Platteville-Galena carbonates within the Kentland impact structure. The shatter cones show evidence of shock metamorphism. 9

Figure 3: Stratigraphic column showing the formations which characterize the Kentland impact structure. The oldest exposed unit is the Ordovician Shakopee dolomite, which is part of the Sauk sequence. This is followed by the St. Peter Sandstone and the Platteville-Galena carbonates. Above the carbonates is the Maquoketa shale. The base of this shale is marked by a major marine flooding surface. Near the top of the column is Pleistocene glacial till which unconformably overlies the Paleozoic strata. (Gutschick, 1987) 10

Figure 4: A polymict breccia dike within the Platteville-Galena carbonates. They are irregular to tabular bodies that follow the bedding planes in the crater. The cores within the breccia were drilled for paleomagnetic analysis and are 2.54cm in diameter. The inset photo is a close up of the Polymict breccia. The clasts consist of quartz, dolomite, calcite, sphalerite, monomict breccia fragments and occasional shatter cone fragments. 11

Figure 5: (A) displays an aerial photograph showing the pits at Kentland quarry. The study areas of pit 6 and 7 are highlighted with green and yellow stars respectively (modified after Weber et al., 2018). (B) shows a google map image of pit 6 displaying some of the sites that were drilled in the quarry. Sites were drilled and oriented with a Brunton Compass and an inclinometer. 14

Figure 6: Zijderveld plot of a breccia showing two components. The first component is revealed from 200˚C to 425˚C with a southerly declination and negative inclination, while a higher component is revealed from 600˚C to 650˚C with a northerly declination and positive inclination. 16

Figure 7: A polymict breccia specimen displaying two directions. (A) shows both directions on one Zijderveld plot. Though there is noise, two directions can be picked once isolated to lower temperature components and higher temperature components. (B) shows a northerly and down component from 525˚C to 700˚C, while (C) shows a southerly and up component from 325˚C to 425˚C. These directions appear to be antipodal and may represent magnetization obtained through a reversal. 17

Figure 8: Two Zijderveld plots showing components with a southerly declination and a negative inclination. (A) reveals this component, in a polymict breccia sample, between 200˚C and 400˚C. At temperatures above 425˚C the data becomes noisy and unresolvable. This renders it impossible to unravel the second component

that may be present. (B) shows a similar component, in a host carbonate sample, between 300˚C and 400˚C. Higher temperatures were removed due to noise in the data. 18

Figure 9: Zijderveld plot of an alternating field demagnetization. Between 10mT and 20mT there is an unresolvable component with a northerly declination and positive inclination. From 20mT to 60mT there is a component with a southerly declination and negative inclination. This plot once again reveals two distinct directions appearing in various specimens. 19

Figure 10: : Zijderveld plot showing a polymict breccia specimen with a northerly declination and positive inclination from 100˚C to 350˚C. In (B) higher temperature steps have been removed due to noise, and to better display the northerly component. 20

Figure 11: Zijderveld plots showing components with northerly declinations and positive inclinations. (A) is a Polymict breccia specimen, revealing this direction from 20mT to 120mT. (B) is a host specimen revealing this direction from 20mT to 75mT. 20

Figure 12: Equal area plot showing specimen directions of both the host rock and the polymict breccias. Two distinct groups occur. In the upper hemisphere, the directions consist of specimens with a northerly declination and a positive inclination. This group has an α_{95} of 12 and a k grouping of 6.8. In the lower hemisphere, the specimens consist of a southerly declination and a negative inclination. This group has an α_{95} of 11.5 and a k grouping of 10.6. 22

Figure 13: Equal area plot after the antipodes of the southerly and negative components were calculated. All the directions are in a common hemisphere to determine a mean declination and inclination for all the directions. The α95 in this case is 8.8˚ and the k grouping is 7.6. The mean declination and inclination of the specimens is 7.7˚ and 43.6˚ respectively. 23

Figure 14: (A) Specimens rotated to their tilted position. The grouping (k = 2.14) has a much greater spread than in figure 13, suggesting that the magnetization was acquired after the tilting occurred. The α95 for the tilted specimens is also less significant than the in-situ specimens as it changed from 8.8˚ to 21.1˚. (B) shows %untilting vs. K (grouping). The best grouping is at -1.2% unfolding with K = 7.6 and a declination and inclination of 7.7˚ and 43.6˚ respectively. The tilt test is statistically significant below 35% untilting (McElhinny, 1964). 23

Figure 15: The Apparent Polar Wander Path for North America. The latitude and longitude were calculated from the mean declination and inclination of the specimens as well as the longitude and latitude of the study area. The blue circle on the diagram indicates the time at which the magnetization was acquired. It plots between 190Ma and 200Ma, which indicates that the magnetization was obtained in the Late Jurassic to Early Triassic. (Modified after Torsvik et al., 2012) 24

Figure 16: (A) IRM acquisition curves from both host (blue) and polymict breccia (orange) samples. There is a general concave downward shape with multiple

components existing. The curve begins to saturate around 500mT but increases slightly until reaching full saturation at 2500mT. (B) A representative unmixed IRM acquisition curve of a polymict breccia, showing the three components that best represent the coercivity spectrum. 25

Figure 17: (A-C) show representative triaxial thermal demagnetization plots from one host specimen and two breccia specimens respectively. Unblocking temperatures range from 450˚C to 550˚C, and is consistent with a low coercivity mineral like magnetite. The Z-axis in C shows decay closer to 575˚C which could be indicative of a higher coercivity mineral like hematite. All 3 axes in C tend to increase at temperatures above 600˚C and could represent the formation of new magnetic minerals. 27

Figure 18: (A) Photomicrograph showing the Platteville-Galena carbonate host rock in plane light. (B) Photomicrograph an echinoderm being partially replaced by silica in cross polarized light. 28

Figure 19: (A) Photomicrograph showing dissolution of the matrix as well as complete dissolution of some dolomite rhombs in plane light. The dissolved rhombs are surrounded by a fibrous rim with some porosity. (B) SEM image of dolomites with dissolution of a ferroan rim and partial dissolution of the rhomb in the center. 29

Figure 20: Photomicrographs showing calcite veining in cross polarized light. (A) Sparry calcite veins present within a host specimen, while (B) shows twinning of calcite within a vein. 29

Figure 21: Photomicrograph showing a secondary calcite vein associated with a hydrothermal phase of baroque dolomite within the transition zone in (A) plane light and (B) cross-polarized light. 30

Figure 22: (A) and (B) show SEM backscatter images of the suevite-like flow. Note the alignment of the phases present such as illite clays (Cl), pyrite (Py), apatite (Ap), gypsum (Gyp), dolomite (Dol) and calcite (Ca). The apatite and gypsum occur as elongate bodies within the flow suggesting they are authigenic. Some apatite in (B) appears more tabular in shape. 30

Figure 23: Magnetic phases present in the transition zone. (A) A backscatter SEM image of a pyrite grain being partially replaced by magnetite along with some pyrite framboids being replaced by magnetite. (B) A backscatter SEM image of a pyrite framboid being partially replaced by an iron oxide with a hint a silica, indicating it may be goethite. (C) A backscatter SEM image of an iron oxide surrounded by clays. (D) A thin section showing a small vein filled with hematite in plane light. 31

Figure 24: (A) shows an SEM backscatter image co-rendered with an elemental map to highlight different phases. The alignment of minerals again suggests a fluidized suevite-like flow. Phases include apatite (Ap), Silica, iron oxides (FeO) and dolomite (Dol). One dolomite clast appears to have been brecciated in place before the flow, allowing the clays and other phases to move through the clast.

(B) Example of authigenic apatite that curves around a silica grain, suggesting precipitation during the flow. 32

Figure 25: (A) Photomicrographs of the Polymict breccias in plane light. The breccias are composed of dolomite crystals and clasts of the host carbonate rock. (B) displays the pervasive vuggy porosity present in the breccias. Upper vugs in the image are spheroidal, while vugs near the bottom of the image keep the shape of the dolomite rhombs that were once there. Some of the dolomite crystals are zoned and, based on EDS analysis, appear to have ferroan rims. 33

Figure 26: Carbonate material with a wispy texture. (A) Photomicrograph showing the calcite with a wispy texture in plane light. (B) Photomicrograph of the calcite being replaced with silica in cross polarized light.....33

Figure 27: (A) Photomicrograph showing a sandstone clast derived from the St. Peter Sandstone in cross polarized light. There is porosity in between the quartz grains that make up the clast. (B) Photomicrograph showing a sphalerite grain in the polymict breccia in plane light. (C) SEM backscatter image of an apatite grain in the polymict breccia. These gains are detrital and were likely brought in from an external source. (D) SEM backscatter image of a coated grain. The grain itself was plucked during the thin section making process. The coating contains clays, dolomite, calcite and euhedral crystals of silica. The inset image shows the hexagonal habit of the silica. This habit points towards it being Tridymite.....34

Figure 28: SEM backscatter images of the magnetic phases present in polymict breccia specimens. (A) Pyrite grain being replaced by magnetite. (B) Gypsum rosettes that have been replaced by hematite. (C) hematite occurring as a cement between the silica grains and carbonate groundmass.....35

Introduction

Many meteorite impacts are not well dated, in fact less than 50% of known terrestrial impacts have been dated as of 1996 (Grieve and Pesonen, 1996). The age and timing of impacts is important because certain impact events can be linked together and some can be tied to geologic events like extinctions (Jourdan et al., 2012; Bottomley et al., 1978). Stratigraphic constraints can be used to date impacts; however, they commonly give a large range for the potential age of an impact (Laney and Van Schmus, 1978). Radiometric age dating techniques, such as K-Ar dating, is the most common method used to acquire an absolute date for impact craters, however, the dates obtained are prone to large errors as clasts in the impact melts and breccias may contain inherited elements from elsewhere in the rock record (Koeberl and Anderson, 1996).

Paleomagnetism can also provide the timing of an impact, as impact melt and breccias can be directly sampled and dated by comparison of pole positions for magnetizations with well-established apparent polar wander paths (e.g., Urrutia-Fucugauchi et al., 2004; Reynolds et al., 1997; and numerous others). Rocks at impact sites can contain remagnetizations due to heating (thermoremanent magnetization), chemical alteration (Chemical remanent magnetization), or shock remanent magnetization (SRM) (Pilkington, 1992). A shock remanent magnetization can be obtained during the passing of a low-pressure shockwave, but is not common (Cisowski and Fuller, 1978). Chemical remanent magnetizations can be acquired during the passage of hydrothermal fluids like water released from target rocks and local brines that can precipitate ferromagnetic minerals after the impact (Fairchild et al., 2016). Thermoremanent magnetizations can be acquired by breccias directly, via frictional heating, during emplacement when the impact occurs (Fairchild et al., 2016 & Halls, 1979). The latter two mechanisms are the more common cause of stable remagnetizations in impact rocks (Urrutia-Fucugauchi et al., 2004 & Elmore & Dulin, 2007).

A number of studies have conducted paleomagnetic analysis directly on impact breccias with promising results. For example, a study on the Bosumtwi impact crater in Ghana, revealed that polymict breccias acquired a stable shock remanence during shock induced grain size reduction (Kontny et al., 2007). Melt rocks collected from the central part of the Lappajärvi crater in Finland revealed a Jurassic thermo-chemical remagnetization (~195Ma) residing in pyrrhotite (Pesonen et al., 1992). Elmore and Dulin (2007) conducted a modified conglomerate test on polymict breccias from the Decaturville impact in Missouri and found a post brecciation CRM with a Permian to Pennsylvanian age. They related the CRM to the passage of hydrothermal fluids. Paleomagnetic analysis of polymict breccias at the Kentland Impact structure also have the potential to date the age of the impact.

The Kentland Impact structure, located at 40˚45'N and 87˚24'W in Newton County, Indiana, is a small complex impact crater (~6km in diameter) that has been partially revealed due to quarrying activities (figure 1). The Kentland Impact structure has 600m of differential uplift, with deformed rocks extending from the Ordovician into the Mississippian, overlain by Wisconsinan glacial till (Gutschick, 1978). These stratigraphic constraints put the age of the Kentland impact between ~325Ma and 50ka.

Jackson and Van Der Voo (1986) conducted a paleomagnetic analysis on 25 Quimby Mills limestone samples at Kentland to gain an estimate of the age of the impact. Thermal demagnetization, with unblocking temperatures up to 300˚C, and alternating field demagnetization (10-30mT) of the samples revealed a Late Cretaceous post tilting magnetization which they interpreted from 4 sites (~25 samples) in the Quimby Mills Limestone formation. The coercivities and maximum unblocking temperatures were relatively low, as were the number of samples analyzed.

In this current study, we conducted a paleomagnetic analysis on the polymict breccia dikes that formed almost contemporaneously with the impact as well as the host carbonates at the Kentland Impact to test the results of the previous study and date the impact.

In addition to knowing the age and timing of an impact it is also important to understand the diagenetic alterations that can result from such an event. During the excavation and modification stages, many of the diagnostic features of an impact begin to form, such as breccias and melt material (French, 1998). As material moves inward and outward, it changes the rock in the vicinity of the impact. Hydrothermal alteration is common after the impact (Osinski et al., 2013; Ames et al., 2006; Hagerty and Newsom, 2003). For example, Pirajno (2009) focuses on the different features produced during the hydrothermal activity associated with impacts. Many impacts, such as the Ries impact structure, have minerals like barite, illite and chlorite, which provide evidence of impact generated hydrothermal fluids (Pirajno, 2009). Through the study of 12 terrestrial impact craters Allen et al., (1982) found that hydrothermal systems generated by an impact event can result in the re-deposition of sulfides in breccias and in fractures. Osinski and Pierazzo (2013) found that almost all complex impact craters have the potential to generate a hydrothermal system.

No previous diagenetic work has been done on the Kentland impact structure and a second objective of this study is to test if the Kentland rocks were altered by hydrothermal fluids that could be related to the impact. This was accomplished by conducting a petrographic and scanning electron microscopy study on samples from the crater. We also tested for the presence of mineral assemblages and alteration that is indicative of a hydrothermal system, as well as characterize the overall diagenetic evolution of the rocks within the impact crater.

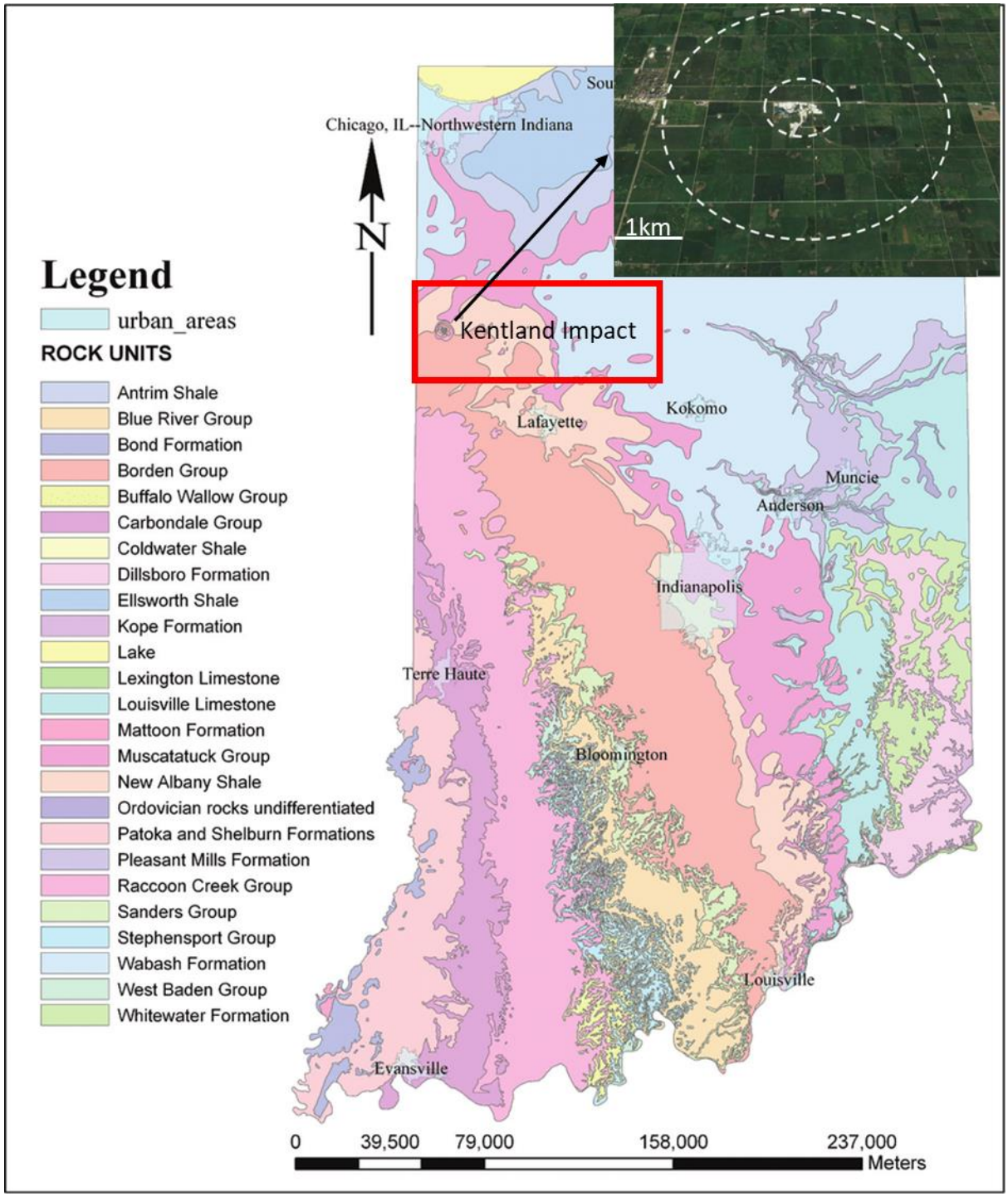

Figure 1: The Kentland impact structure, highlighted in the red box, is located at 40°45'N and 87°24'W in Newton County, Indiana (Modified after Gray, 1989). It is a small complex crater that is ~6Km in diameter. The inset shows the approximate size of the crater (Modified after United States Meteorite Impact Craters, 2017).

Geologic and Tectonic Background

According to French (1998), hypervelocity impacts generally have three phases: the contact and compression stage, the excavation stage and the modification stage. The first phase refers to the initial impact of the meteor and the high-pressure shock waves that develop (French, 1998). This happens in a matter of seconds, and grades into the second stage in which interactions from the shock wave drives rock outward to produce a flow upward in the center of the structure. The flow is symmetric and produces the characteristic bowl-shaped transient crater. This stage ranges from seconds to a few minutes (French, 1998). Once the crater has ceased growing, the last stage is characterized by gravity flow processes and natural processes such as uplift, mass movement, erosion and sedimentation (French, 1998).

The 160,000m^2 Kentland Quarry contains part of the centrally uplifted section of the Kentland impact structure (Gutschick, 1972). Although the nature of this structure has been highly debated (Collett, 1883; Gorby 1886; Ward, 1906; Chamberlin, 1923; Cummings and Shrock, 1928), there are multiple lines of evidence that suggest the Kentland structure is the result of an impact. The quarry contains evidence of shock metamorphism such as shatter cones (figure 2) (Dietz, 1947;1960), impactites (French, 1998), polymict breccia dikes (Bjørnerud, 1998), coesite (Cohen et al, 1962; though this result has not proven reproducible), feather structures (Morrow and Weber, 2009) and brittle quartz microstructures (Laney and Van Schmus, 1978). Furthermore, based on a geochemical study and, comparing the breccias to the source carbonates, Koeberl and Sharpton (1993) report the breccias contained a weak cosmic component of 0.02%, due to approximately 0.15ppb of Iridium, compared to the undeformed carbonates. The Kentland structure is highly eroded, and there are no visible impact melt deposits present.

Within the Kentland structure, rocks are extensively faulted and folded with some layers tilted to near vertical (Bjørnerud, 1997). In contrast, surrounding the crater, the Paleozoic strata dip gently toward the Illinois basin (Laney and Van Schmus, 1978). The bedrock within the crater has been uplifted by approximately 600m (Gutschick, 1972, 1978), which in turn has exposed more than 300m of stratigraphic section consisting of carbonate, sandstone and shale formations (Laney and Van Schmus, 1978). Based on statistical relations (Grieve et. al, 1981; Grieve and Pilkington, 1996) and empirical relations (Melosh and Ivanov, 1999), the amount of stratigraphic uplift seen within an impact is equal to approximately 10% of the diameter of the crater. As a result, the 600m of uplift within the Kentland impact structure puts its diameter at approximately 6km.

The Kentland impact structure is bounded to the north by the Michigan Basin and the Kankakee Arch and bounded to the south and west by the Illinois Basin (Collinson et al., 1988). The Paleozoic sequences at Kentland were deposited in the Illinois basin, which extends into southwestern Indiana. Near the end of the Precambrian the New Madrid Rift complex developed resulting in extensional faulting and subsidence (Kolata and Nelson, 1990), which lead to the formation of the Illinois basin. On top of the Precambrian basement, a major marine transgression (Kolata and Nelson, 1990) resulted in the deposition of the Ordovician Shakopee Dolomite, which is the oldest unit exposed at Kentland (figure 3). The Ordovician St. Peter sandstone overlies the Shakopee Dolomite. Weber et al. (2005) used detrital apatite found in the St. Peter sandstone as part of an apatite fission track study, which dated a Jurassic regional exhumation event. Above the sandstone, is the Middle - Late Ordovician Platteville and Galena carbonate groups (Sloss, 1963) (figure 3). Near the top of this group, the Quimby Mills Limestone was deposited. In the Late Ordovician, the Taconic orogeny resulted in increased sedimentation of siliciclastics, which

consequently led to the deposition of the Maquoketa Shale (Kolata and Nelson, 1990). At the base of the Maquoketa shale unit, there is a distinct horizon marked by a major flooding surface with pyritized bone fragments (figure 3) (Gutschick, 1972). In parts of the quarry, the youngest exposed strata are the Lower to Middle Silurian Sexton Creek and Salamonie formations. Surrounding the quarry, Pennsylvanian sandstones overlie the older horizons and the Paleozoic strata are unconformably overlain by Pleistocene (<50ka) glacial till (Gutschick, 1987;1983).

Within the exposed section of the Platteville–Galena carbonate group, numerous impact-related breccias are found. Bjørnerud (1997) defined three types of breccias at Kentland. Fault breccias are usually monomict and contain the coarsest clasts. Breccia lenses have clasts 2-3mm in size and are better sorted than the fault breccias (Bjørnerud, 1997). Breccia dikes are polymict in nature, can be centimeters to meters in length, and tend to cross cut the other types of breccias (figure 4) (Bjørnerud, 1997). The polymict breccias are irregular to tabular and follow the bedding planes and fault surfaces that are present in the crater (Laney and Van Schmus, 1978). The polymict breccias contain clasts from the lithologies present in the stratigraphic section including quartz, chert, dolomite, calcite, shale, monomict breccia fragments and occasional shatter cone segments (Laney and Schmus, 1978).

One of the principal faults bounding the centrally uplifted part of the crater is the Kentland Quarry Fault (Gutschick, 1987). It is a steeply dipping, folded, reverse fault that places the St. Peter sandstone against the Platteville-Galena Carbonate group (Gutschick, 1987). This fault becomes a normal fault when the dip direction changes to overturned. In addition to the Kentland Quarry Fault, there are numerous radial faults (Gutschick, 1978). These faults radiate from the peak of the structure, and similar features called radial transpression ridges (RTR) and radial

transtension troughs (RTT) have been found in other impact structures (Kenkmann and Dalwigk, 2000).

Alder et al. (2017) studied these radial faults within the Kentland impact structure and found fault groups within the various pits in the quarry that likely formed during the cratering event. These normal and reverse faults define large wedges of rock, some of which open inward toward the peak of the uplift, and some of which open outward and away from the peak (Alder et al., 2017). The outward opening wedges are consistent with radial transtension troughs identified by Kenkmann and Dalwigk (2000) and most probably occurred during the modification stage of the crater formation, as material flowed outward along steep normal faults (Alder et al., 2017). The inward opening wedges are consistent with radial transpression ridges (Kenkmann and Dalwigk, 2000) and likely formed during the early part of the modification phase as material moved along thrust faults with an inward sense of slip (Alder et al., 2017).

In addition to Jackson and Van Der Voo (1986), Weber et al. (2018) presented preliminary paleomagnetic and petrographic results from polymict breccias at Kentland. This study builds upon the work of those preliminary results.



Figure 2: Shatter cones that have formed within the Platteville-Galena carbonates within the Kentland impact structure. The shatter cones show evidence of shock metamorphism.

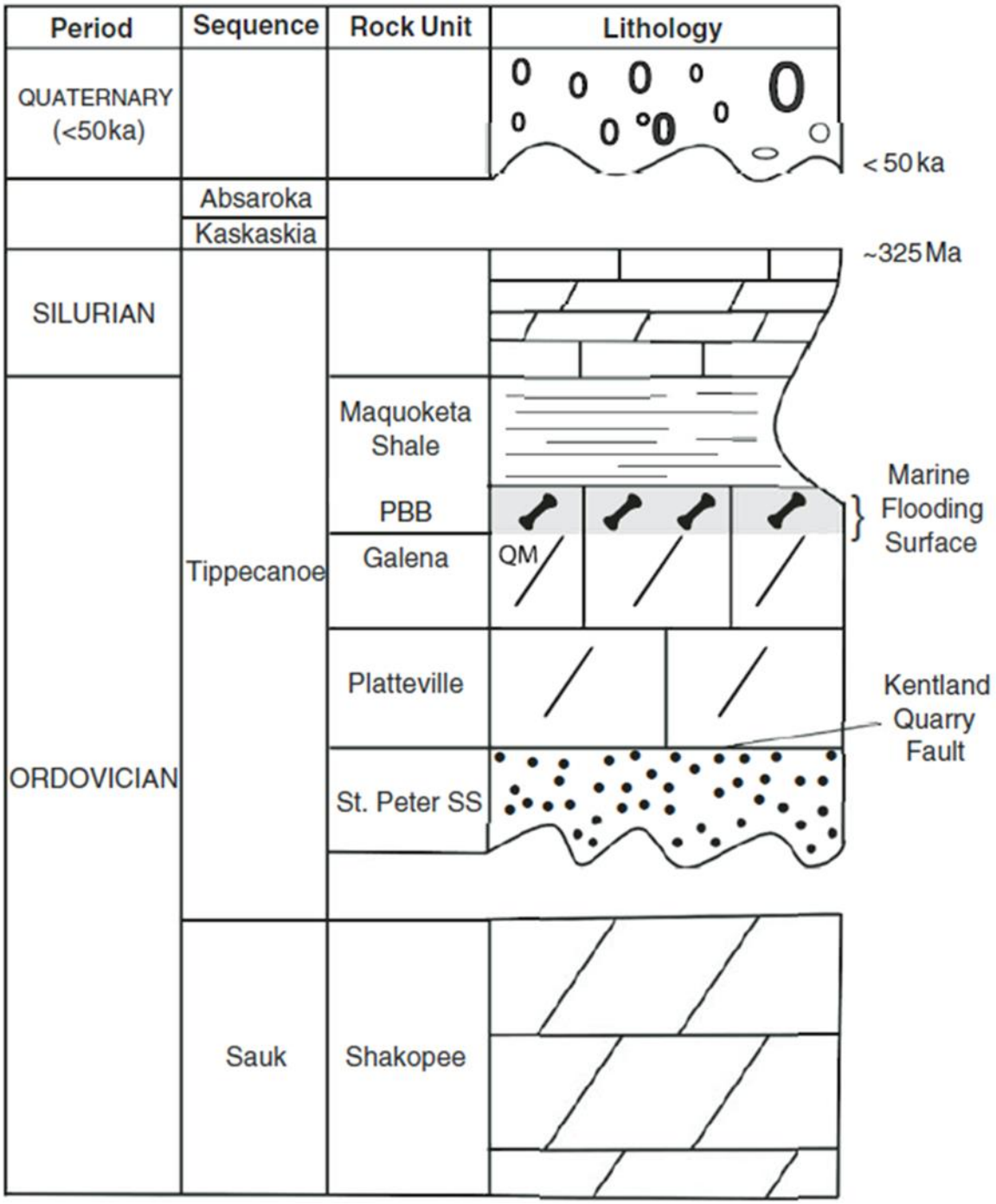

Figure 3: Stratigraphic column showing the formations which characterize the Kentland impact structure. The oldest exposed unit is the Ordovician Shakopee dolomite, which is part of the Sauk sequence. This is followed by the St. Peter Sandstone and the Platteville-Galena carbonates. Above the carbonates is the Maquoketa shale. The base of this shale is marked by a major marine flooding surface. Near the top of the column is Pleistocene glacial till which unconformably overlies the Paleozoic strata. (Gutschick, 1987).



Figure 4: A polymict breccia dike within the Platteville-Galena carbonates. They are irregular to tabular bodies that follow the bedding planes in the crater. The cores within the breccia were drilled for paleomagnetic analysis and are 2.54cm in diameter. The inset photo is a close up of the Polymict breccia. The clasts consist of quartz, dolomite, calcite, sphalerite, monomict breccia fragments and occasional shatter cone fragments.

Methods

Within the Kentland Quarry, we collected cores from polymict breccia dikes as well as the host carbonate rocks using a portable drill. Some sites were collected for a tilt test. Twenty-four sites (13 host and 11 breccia sites), from pits 6 and 7, were drilled and oriented using a Brunton Compass and an inclinometer (figure 5). We cut the cores to standard lengths (2.2cm) for paleomagnetic analysis. We conducted petrographic work on the chips cut form the cores to determine the diagenetic evolution of the rocks within the crater and to test for hydrothermal activity.

The natural remanent magnetizations (NRM) were measured using a 2G Enterprises three-axis cryogenic magnetometer with DC squids. Some specimens were subjected to five low temperature demagnetization (LTD) steps, during which they were placed in liquid nitrogen and allowed to cool to room temperature before measuring the NRM. This allowed zero field cycling between room temperature and the Verwey transition and is effective at removing noise present in the specimens (Dunlop et al., 1997, Warnock et al., 2000, Dunlop, 2003). Selected specimens were subjected to stepwise thermal demagnetization in 19 steps up to 700°C. Other samples were subjected to an alternating magnetic field from 0 to 120mT in increments of 10mT. We displayed these specimen directions on orthogonal projections and straight-line components were selected to identify a characteristic remanent magnetization (ChRM), through principal component analysis, with maximum angular deviation (MAD) values of less than 17° (Kirschvink, 1980). We plotted the chosen components on equal area diagrams and used Fisher (1953) statistics to calculate the mean directions. A tilt test was conducted to determine the timing of the event relative to any tilting that may have occurred. We used the longitude and latitude of the study area along with the mean directions to determine the pole position of the magnetization which was compared to

the North American apparent polar wander path (APWP) (Torsvik et. al, 2012) to evaluate the timing of the magnetization.

Additionally, we conducted isothermal remanent magnetization (IRM) experiments on some specimens by applying a DC field in increasing steps, at room temperature, to each specimen. After each step, the magnetization was measured (Robertson and France, 1993). This allowed for the generation of the IRM acquisition curves which aid in determining the contribution of various magnetic carrier minerals. We analyzed the data using Maxbauer's (2016) Max Unmix program to determine the coercivity spectrum of the specimens, and a Monte-Carlo style calculation was applied for error analysis. The uncertainty for each of the modeled components was displayed via 95% confidence intervals. Thermal demagnetization of triaxial IRMs were also conducted to aid in determining which magnetic carrier minerals were dominant (e.g. Lowrie, 1990). Three IRMs were imparted at 120mT, 500mT and 2500mT.

Over 40 standard polished thin sections were analyzed from the host carbonate material as well as the polymict breccia sites in order to identify phases and develop paragenetic sequences for the breccias and host carbonate. Petrographic analysis was conducted on a Zeiss Axio Imager.Z1m microscope, to infer the mineralogy and observe textures present in the thin sections. Once key features were identified, the thin sections were then analyzed using a FEI Quanta 250 scanning electron microscope (SEM) fitted with a Bruker XFlash 6I100 energy dispersive spectroscopy (EDS) attachment to allow for identification of the components in the samples. The system was operated at an accelerating voltage between 15kV and 25kV with a spot size of 5. The working distance of the stage to the beam was between 5mm and 10mm.

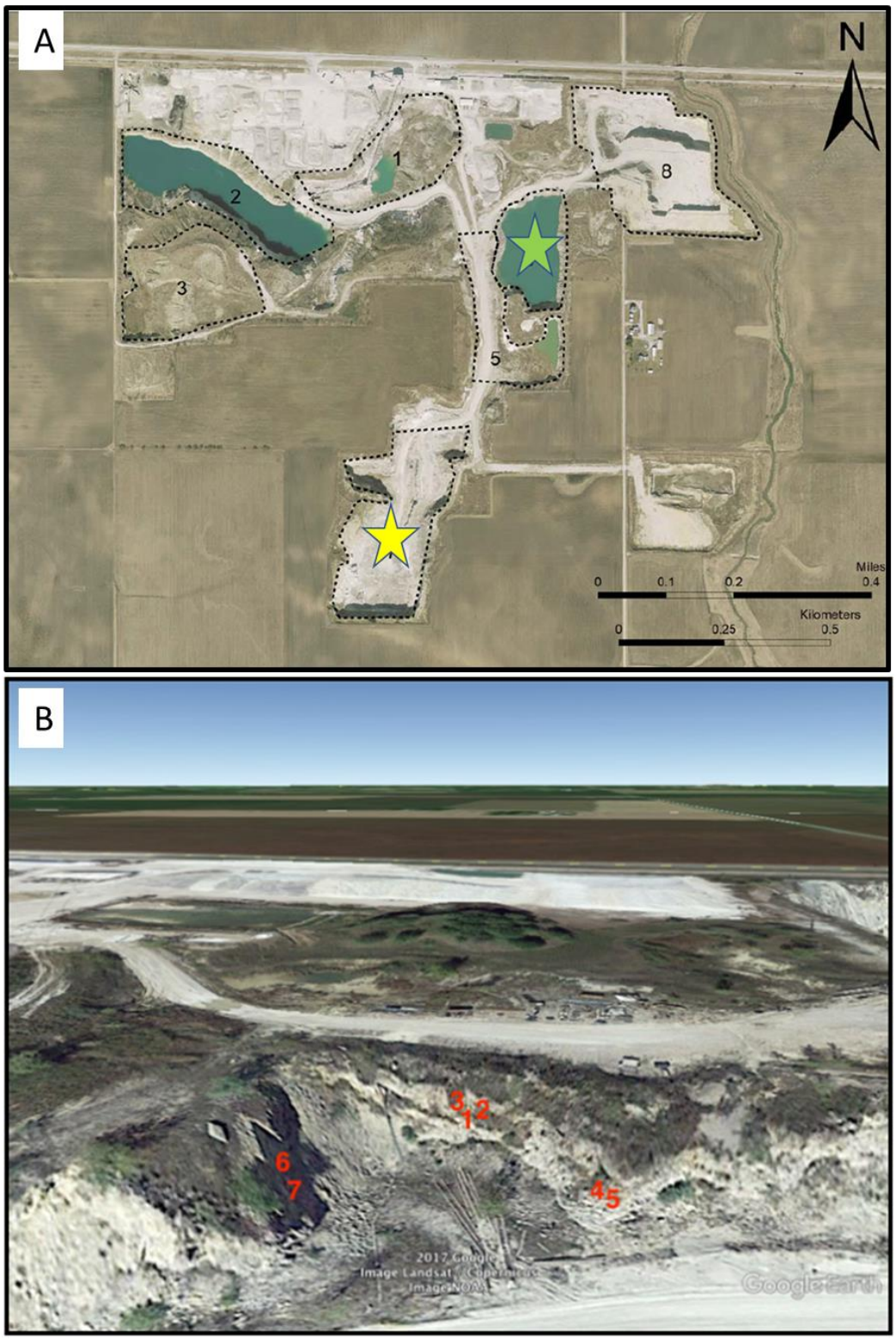

Figure 5: (A) displays an aerial photograph showing the pits at Kentland quarry. The study areas of pit 6 and 7 are highlighted with green and yellow stars respectively (modified after Weber et al., 2018). (B) shows a google map image of pit 6 displaying some of the sites that were drilled in the quarry. Sites were drilled and oriented with a Brunton Compass and an inclinometer.

Results and Interpretations

Paleomagnetism

Thermal and alternating field demagnetization were conducted on 104 specimens. The mean NRM intensity of the specimens is 0.018 ± 0.02mA/M. Of the 104 specimens, 10 were selected for a pilot run of LTD. The average drop in the NRM magnetic intensity after conducting 5 LTD steps was 0.002 ± 0.001mA/M. The addition of these low temperature steps did not noticeably aid in cleaning up the components of magnetization, so it was not applied to the rest of the specimens.

The room temperature thermal and alternating field demagnetization conducted on both the host and polymict breccia specimens revealed two major components; one with southerly declinations and negative inclinations, and the other with northerly declinations and positive inclinations. Some specimens contained both components while others revealed only one. As such, the results presented below are broken into 3 main categories: specimens with two components, specimens with southerly and up components and specimens with northerly and down components. A viscous remanent magnetization (VRM) is not well defined in most specimens.

Specimens with Two Components

Thermal demagnetization of some polymict breccia specimens reveal two distinct directions (figure 6). No host carbonate samples contained two components. Additionally, alternating field demagnetization did not reveal specimens with two components. Southerly declinations and negative inclinations are revealed at lower temperatures (200˚C to ~425˚C), while

northerly declinations with positive inclinations are revealed in three specimens at higher temperatures (~450˚C up to 700˚C).

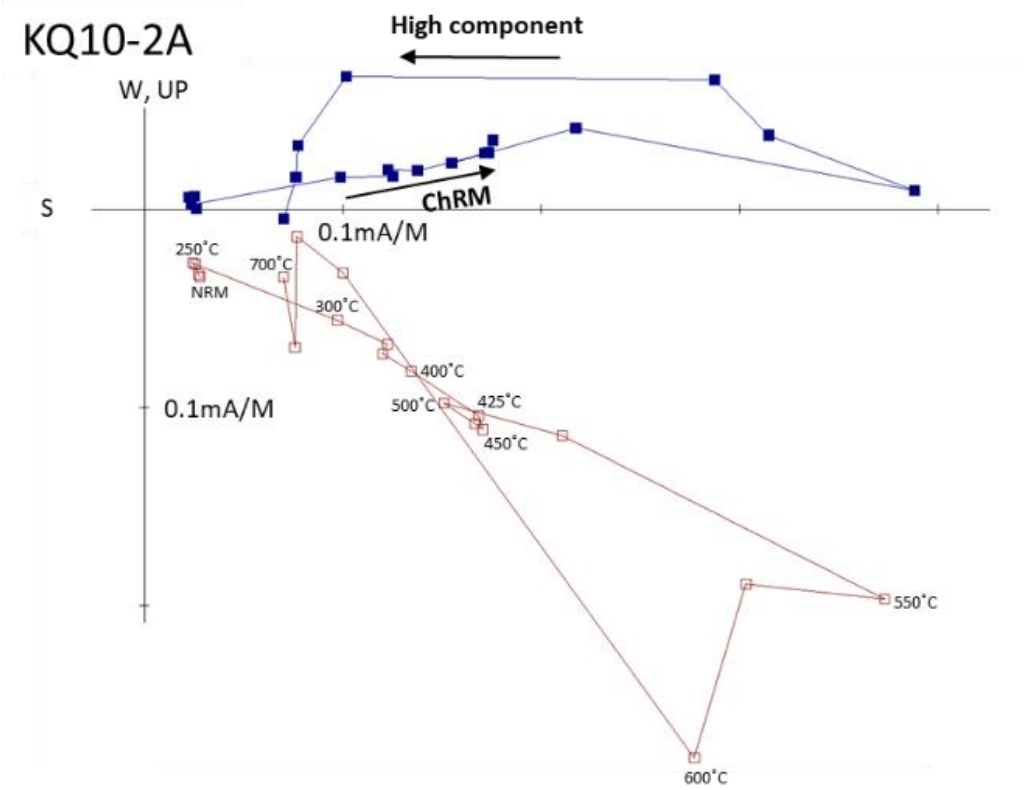

Figure 6: Zijderveld plot of a breccia showing two components. The first component is revealed from 200˚C to 425˚C with a southerly declination and negative inclination, while a higher component is revealed from 600˚C to 650˚C with a northerly declination and positive inclination.

The magnetic intensities of these specimens increase before decreasing to a minimum. (figures 6 & 7). As the lower temperature component is unraveled, the second component begins to reveal itself causing the overall intensity in the specimen to increase. After the lower temp component is fully removed, the second higher temperature component is removed.

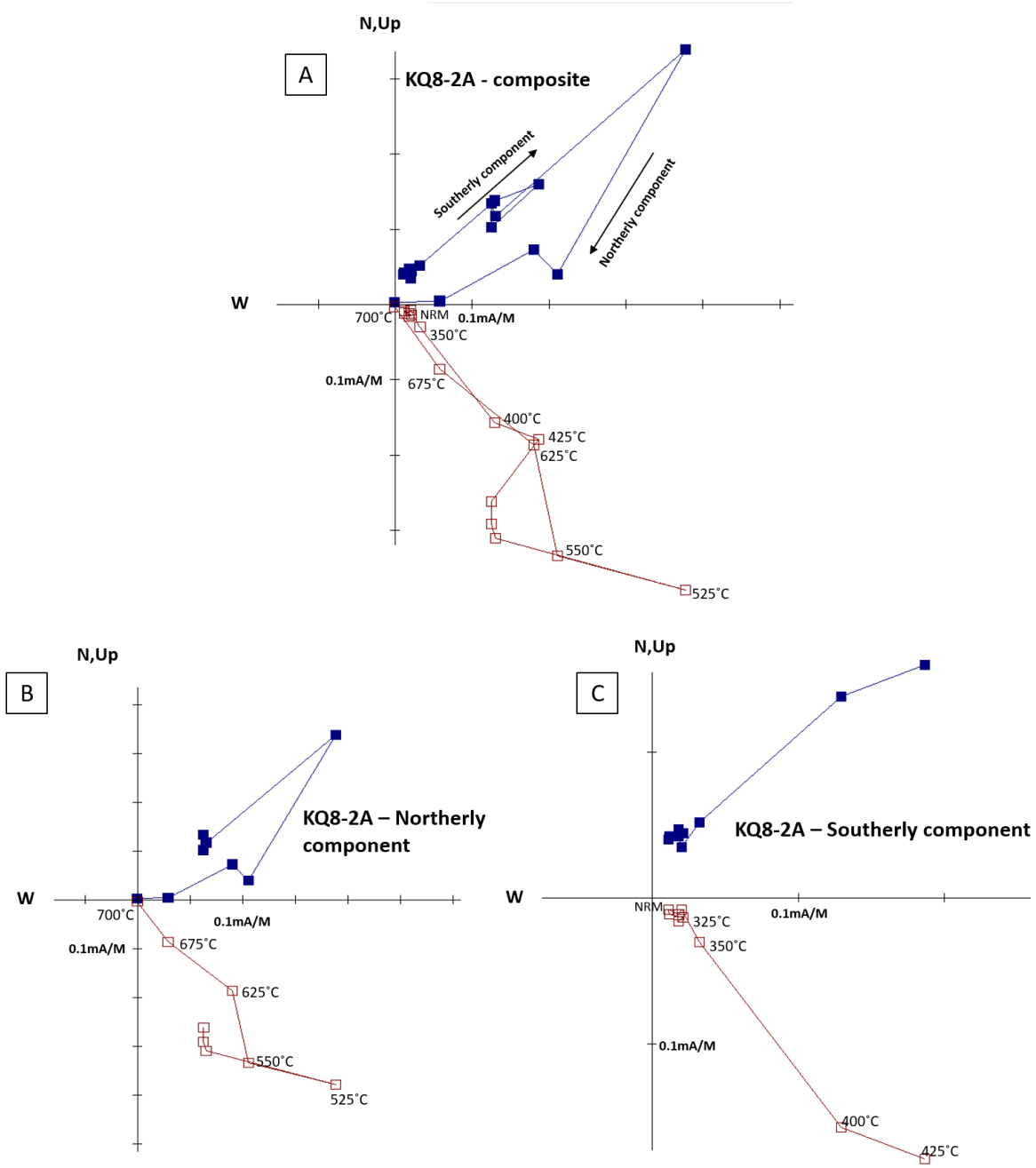

Figure 7: A polymict breccia specimen displaying two directions. (A) shows both directions on one Zijderveld plot. Though there is noise, two directions can be picked once isolated to lower temperature components and higher temperature components. (B) shows a northerly and down component from 525˚C to 700˚C, while (C) shows a southerly and up component from 325˚C to 425˚C. These directions appear to be antipodal and may represent magnetization obtained through a reversal.

Specimens with Southerly and Up Component

Thermal demagnetization of some host and polymict breccia specimens, reveal one distinct direction with southerly declinations and negative inclinations between 200˚C and 400˚C (figure 8A & 8B). Two specimens had higher temperature components from 475˚C to 650˚C. In these specimens, the northerly component is either absent or unresolvable due to noise. In some specimens the magnetic intensity increases but never decreases in a consistent pattern, as the decay pattern becomes too noisy to resolve (figure 8B). Alternating field demagnetization also reveals this component, with southerly declinations and negative inclinations (figure 9).

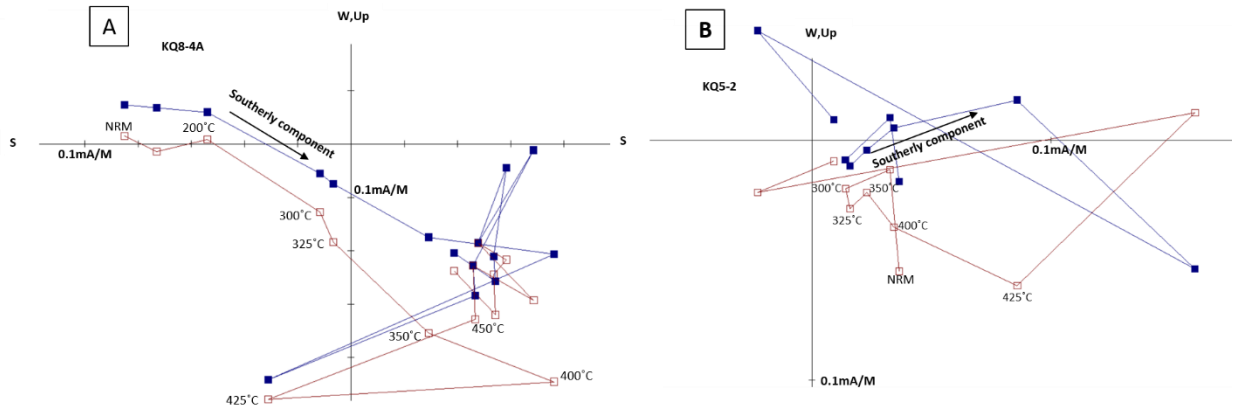

Figure 8: Two Zijderveld plots showing components with a southerly declination and a negative inclination. (A) reveals this component, in a polymict breccia sample, between 200˚C and 400˚C. At temperatures above 425˚C the data becomes noisy and unresolvable. This renders it impossible to unravel the second component that may be present. (B) shows a similar component, in a host carbonate sample, between 300˚C and 400˚C. Higher temperatures were removed due to noise in the data.

Alternating field demagnetization of the polymict breccias does not isolate both components. Figure 9 shows a northerly and down direction at low field strengths, a possible VRM, and a component with a southerly declination and a positive inclination from 20 mT to 60mT.

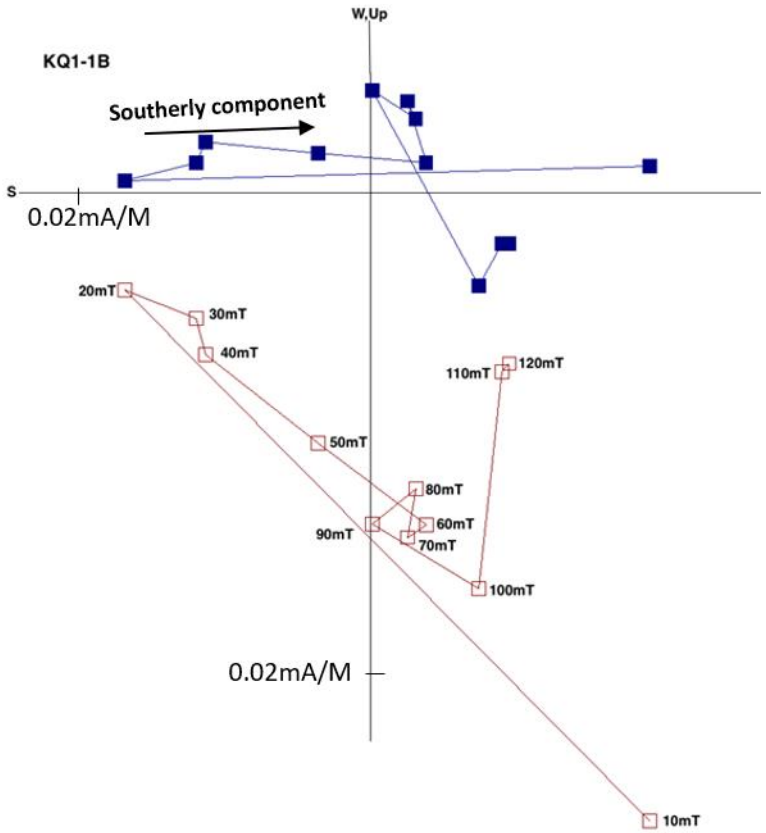

Figure 9: Zijderveld plot of an alternating field demagnetization. Between 10mT and 20mT there is an unresolvable component with a northerly declination and positive inclination. From 20mT to 60mT there is a component with a southerly declination and negative inclination. This plot once again reveals two distinct directions appearing in various specimens.

Specimens with Northerly and Down Component

Thermal demagnetization of some polymict breccia specimens revealed a single component with northerly declinations and positive inclinations. Figure 10 shows a Zijderveld plot of the specimen along with a blown up inset, showing the northerly component which exists from 100˚C to 350˚C.

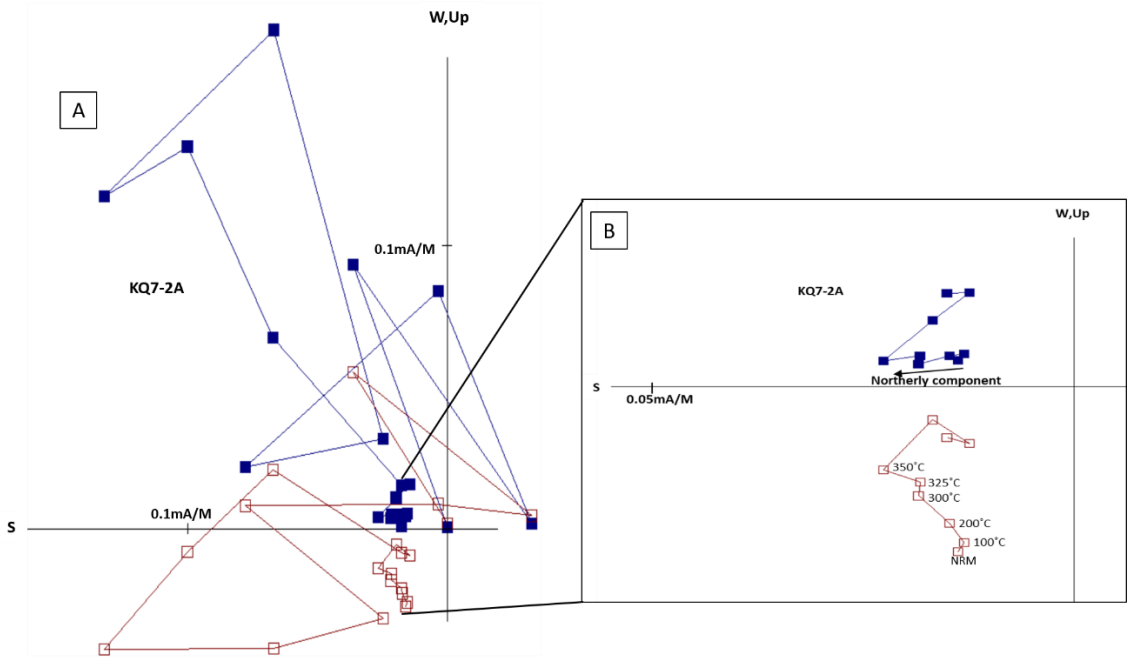

Figure 10: Zijderveld plot showing a polymict breccia specimen with a northerly declination and positive inclination from 100˚C to 350˚C. In (B) higher temperature steps have been removed due to noise, and to better display the northerly component.

Alternating field demagnetization of both polymict breccia and host specimens also reveal a northerly component with positive inclinations from 20mT to 75mT (figure 11A & 11B).

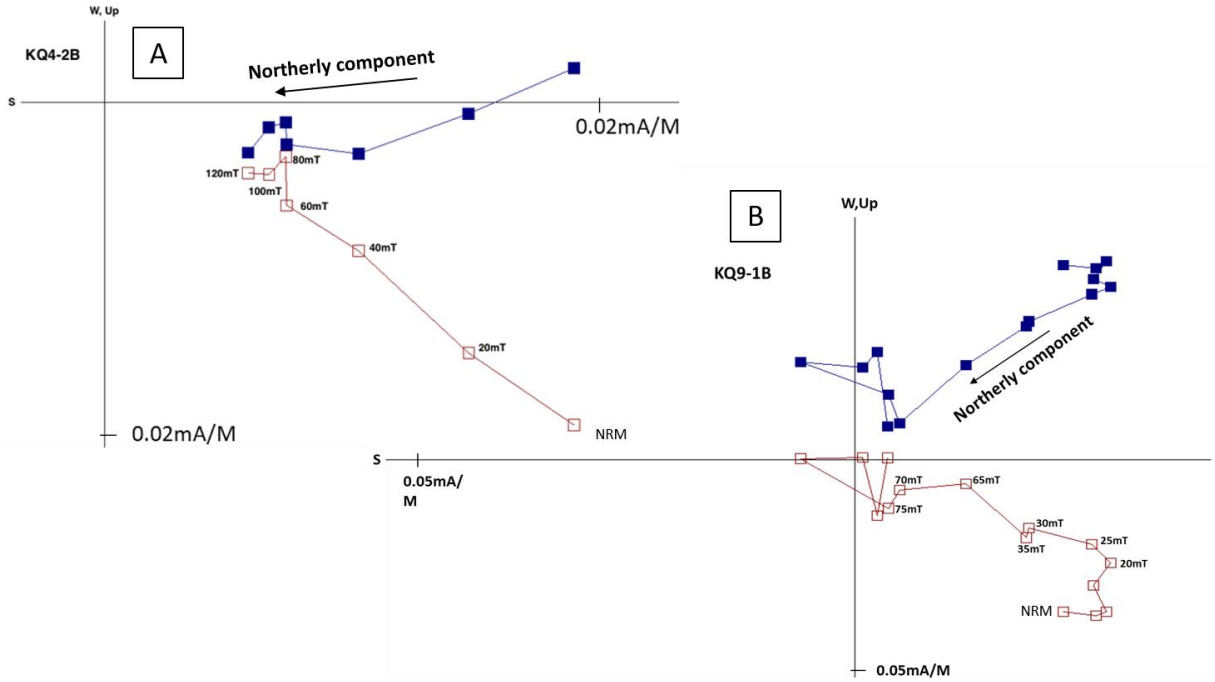

Figure 11: Zijderveld plots showing components with northerly declinations and positive inclinations. (A) is a Polymict breccia specimen, revealing this direction from 20mT to 120mT. (B) is a host specimen revealing this direction from 20mT to 75mT.

Analysis of Specimen Directions

After analysis, 34 out of 104 specimens were found to be interpretable with mean angular deviation (MAD) values of less than 17˚ (figure 12). There were a few more interpretable samples, however, the MAD values were over 17˚ and were not used in the analysis for this study. These results are similar to those obtained by Jackson and Van Der Voo (1986), who sampled two or three sites from 8 formations but only found a stable magnetization with consistent directions in six sites (~30 specimens) from the Quimby Mills Limestone within the crater. The specimens from the Kentland crater have low NRMs and display noisy decay. The 34 successful specimens have an average NRM intensity of 0.027 ± 0.03mA/M, whereas the remaining unsuccessful specimens have an average NRM intensity of 0.013 ± 0.01mA/M. This trend indicates that the strength of magnetization plays a role in the presence of the characteristic directions.

Of the 34 specimens with good components, 21 were polymict breccia specimens while 13 were host carbonate specimens. On average the NRM intensities of the 23 breccias (0.032 ± 0.04mA/M) are twice as much as the 13 host carbonates (0.015 ± 0.02mA/M), showing that the polymict breccias provide more robust data than the host carbonate alone. Since the number of successful specimens are low, site means were not statistically possible as there were only 2 to 3 specimens per site with stable magnetizations. As such, the data below are presented as specimen directions rather than site means.

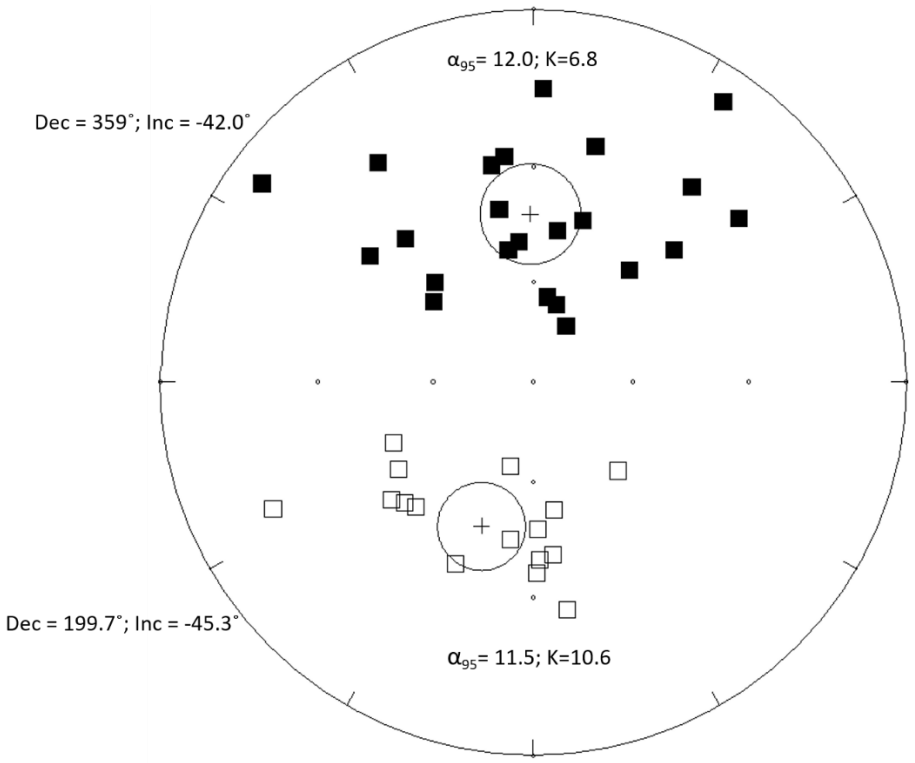

Figure 12: Equal area plot showing specimen directions of both the host rock and the polymict breccias. Two distinct groups occur. In the upper hemisphere, the directions consist of specimens with a northerly declination and a positive inclination. This group has an α_{95} of 12 and a k grouping of 6.8. In the lower hemisphere, the specimens consist of a southerly declination and a negative inclination. This group has an α_{95} of 11.5 and a k grouping of 10.6.

Two distinct groupings of specimen directions can be seen in the equal area plot (figure 12). These groups appear to be antipodal in nature and a reversal test (McFadden and Lowes, 1981) shows that the two directions share a common mean at the 95% confidence level. Since these directions are antipodal to one another, we reversed the components with southerly declinations and negative inclinations to bring all the points to a common hemisphere (figure 13). The mean declination is 7.7˚ and inclination is 43.6˚ (cone of 95% confidence [α_{95}] = 8.8˚; k [grouping] = 7.6). In addition, a tilt test indicated that the best grouping is in the in-situ direction (figure 13) compared to the tilted direction (figure 14). As a result, the magnetization was acquired after tilting occurred.

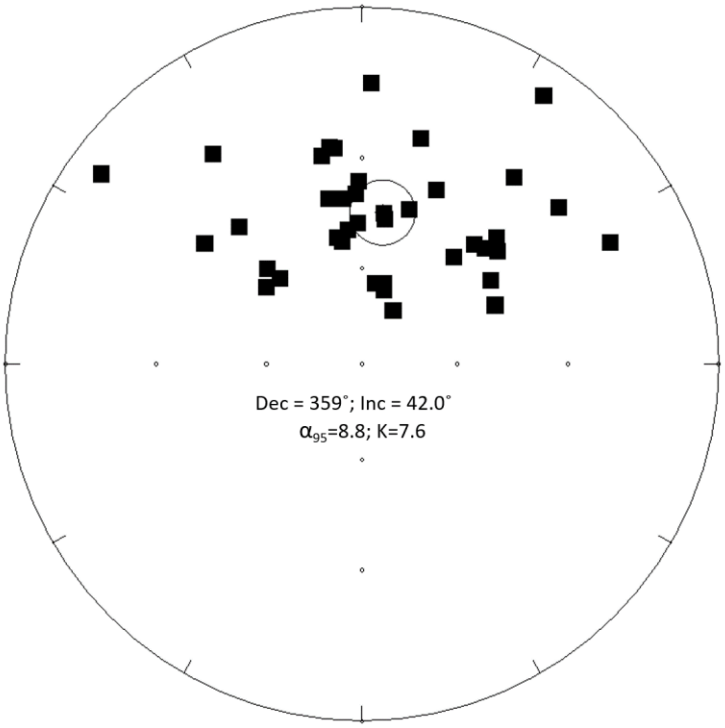

Figure 13: Equal area plot after the antipodes of the southerly and negative components were calculated. All the directions are in a common hemisphere to determine a mean declination and inclination for all the directions. The α95 in this case is 8.8˚ and the k grouping is 7.6. The mean declination and inclination of the specimens is 7.7˚ and 43.6˚ respectively.

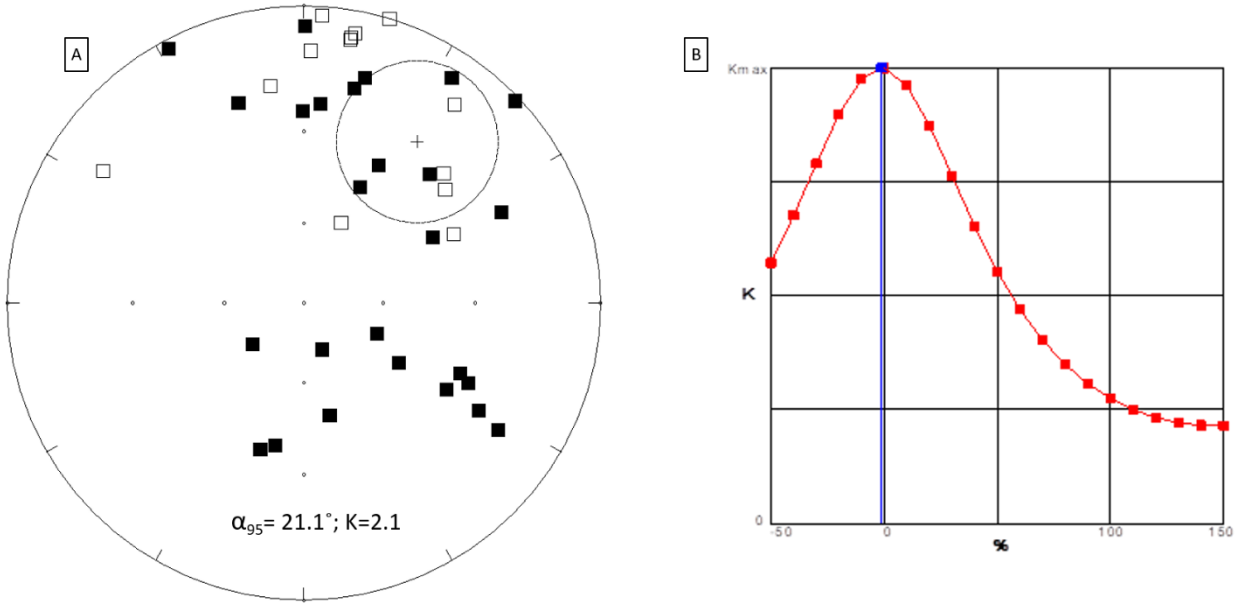

Figure 14: (A) Specimens rotated to their tilted position. The grouping (k = 2.14) has a much greater spread than in figure 13, suggesting that the magnetization was acquired after the tilting occurred. The α95 for the tilted specimens is also less significant than the in-situ specimens as it changed from 8.8˚ to 21.1˚. (B) shows %untilting vs. K (grouping). The best grouping is at -1.2% unfolding with K = 7.6 and a declination and inclination of 7.7˚ and 43.6˚ respectively. The tilt test is statistically significant below 35% untilting (McElhinny, 1964).

We used the mean in situ direction to calculate the pole position of the magnetization which has a latitude of 73.4˚N and a longitude of 67.6˚E (dp/dm [semi-axes of the oval of 95% confidence around the poles] = 6.8˚/11.0˚). The pole plots near the Late Triassic – Early Jurassic part of the Apparent Polar Wander Path for North America between 190Ma and 200Ma (figure 15).

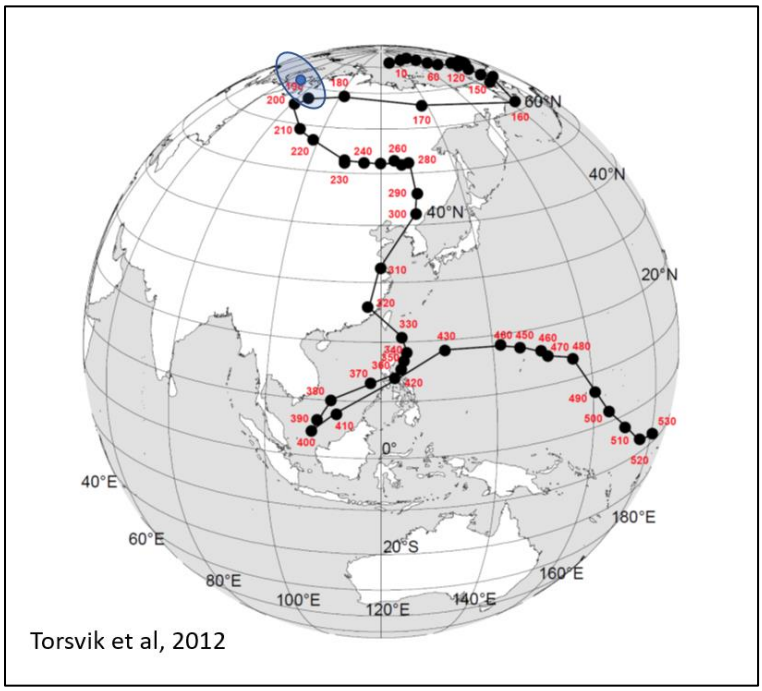

Figure 15: The Apparent Polar Wander Path for North America. The latitude and longitude were calculated from the mean declination and inclination of the specimens as well as the longitude and latitude of the study area. The blue circle on the diagram indicates the time at which the magnetization was acquired. It plots between 190Ma and 200Ma, which indicates that the magnetization was obtained in the Late Jurassic to Early Triassic. (Modified after Torsvik et al., 2012)

Rock Magnetism

IRM Acquisition

IRM acquisition experiments were conducted on both host carbonate and polymict breccia specimens. Representative acquisition curves started to flatten at about 400 mT and increased slightly up to 2500mT (figure 15A). This suggests the magnetization is dominated by a low coercivity phase followed by a higher coercivity phase. IRM unmixing models suggest that the coercivity spectrum is represented by three components (figure 15B) with mT ranges of 1.8mT,

2.1mT and 3.4mT. These are consistent with values reported for magnetite, hematite and goethite, respectively (Egli, 2003).

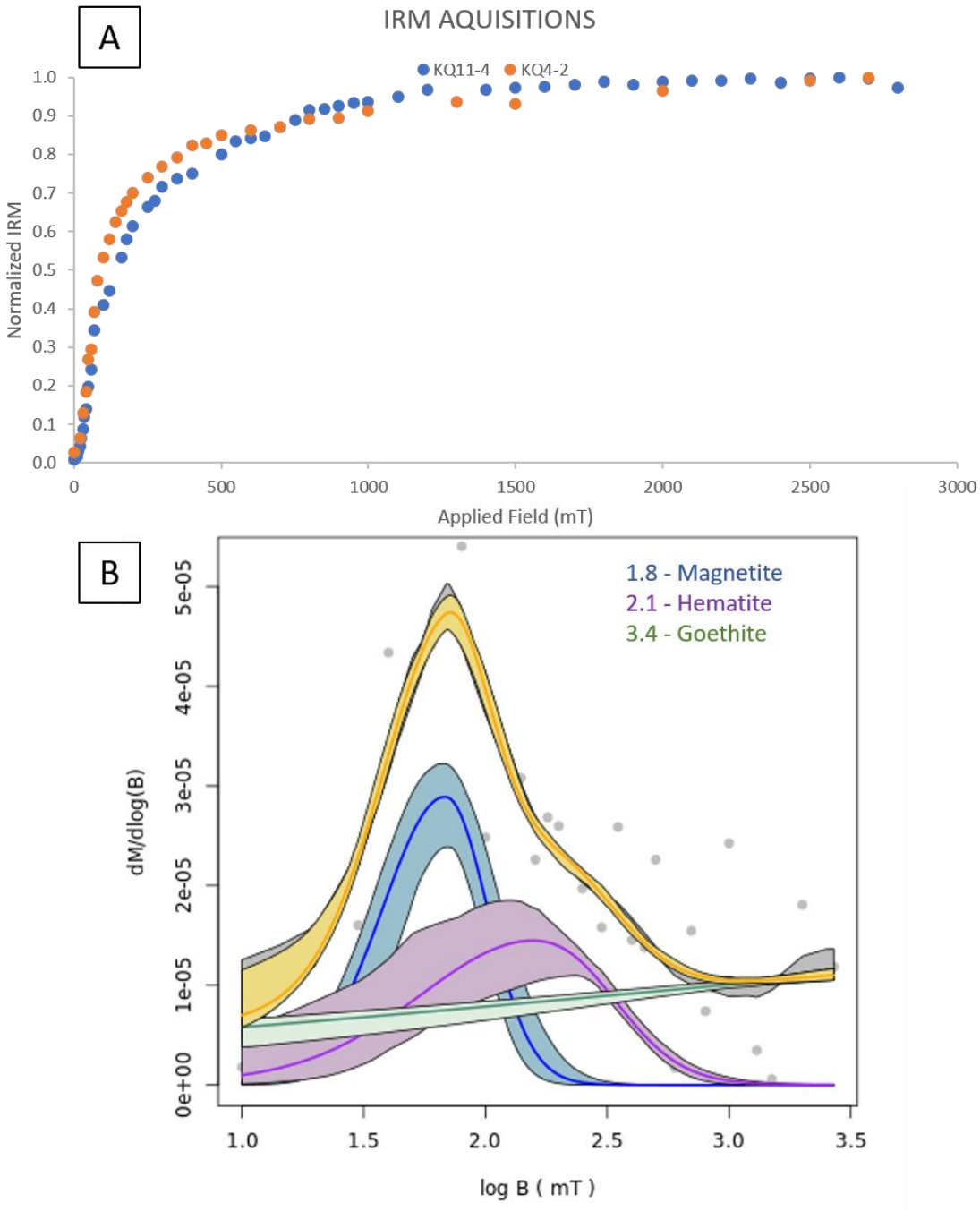

Figure 16: (A) IRM acquisition curves from both host (blue) and polymict breccia (orange) samples. There is a general concave downward shape with multiple components existing. The curve begins to saturate around 500mT but increases slightly until reaching full saturation at 2500mT. (B) A representative unmixed IRM acquisition curve of a polymict breccia, showing the three components that best represent the coercivity spectrum.

Triaxial Thermal Decay

Triaxial thermal demagnetization was conducted on both the host as well as the polymict breccias and representative plots are shown in figure 17. The 120 mT component is dominant for both breccias and host carbonate specimens. The maximum unblocking temperatures is 450˚C to 550˚C, which is consistent with magnetite (figure 17A&B). The magnetization tends to increase at temperatures above 600˚C, which can be attributed to the creation of new magnetic minerals (figure 17C).

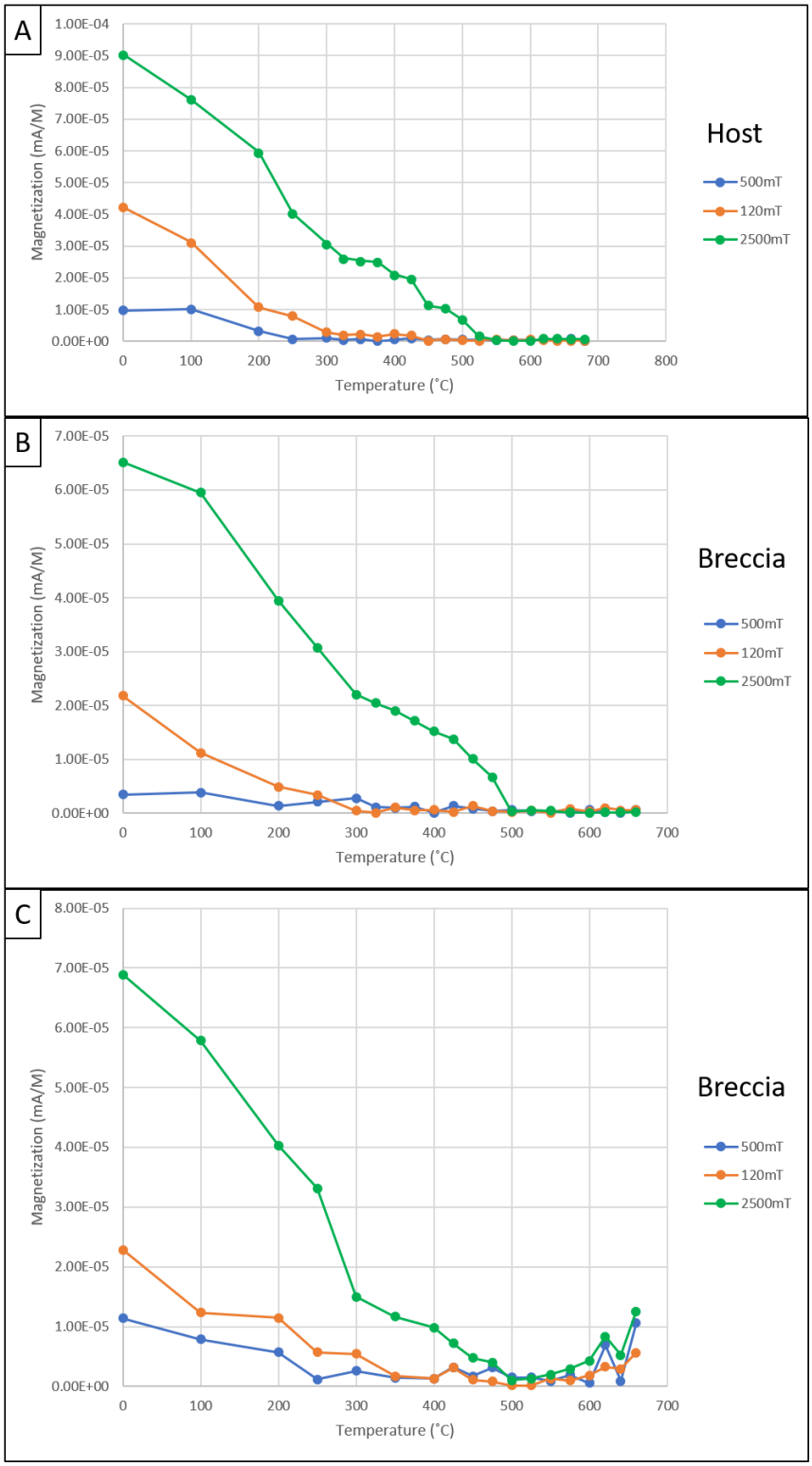

Figure 17: (A-C) show representative triaxial thermal demagnetization plots from one host specimen and two breccia specimens respectively. Unblocking temperatures range from 450˚C to 550˚C and is consistent with a low coercivity mineral like magnetite. The Z-axis in C shows decay closer to 575˚C which could be indicative of a higher coercivity mineral like hematite. All 3 axes in C tend to increase at temperatures above 600˚C and could represent the formation of new magnetic minerals.

Diagenesis

Diagenesis of the Host Carbonates

The host carbonates of the Platteville-Galena Group are classified as wackestones to packstones. They contain numerous allochems such as crinoids, bryozoans, mollusks, brachiopods and trilobites (figure 18A). Some rocks are completely dolomitized whereas some contain only minor dolomite. Some allochems have been partially to completely replaced by silica (figure 18B). The matrix consists mainly of micrite, calcite cement, calcite clasts and dolomite.

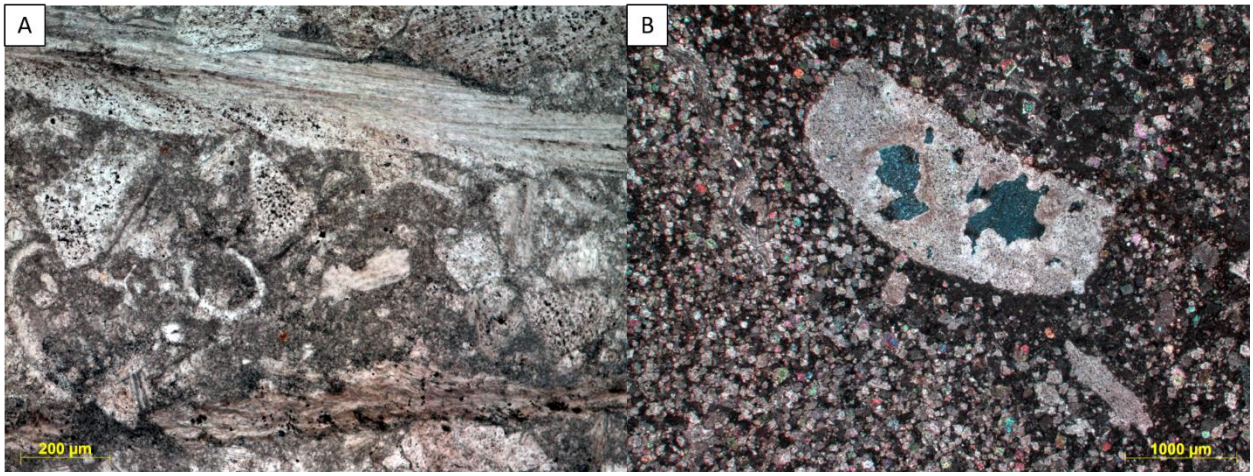

Figure 18: (A) Photomicrograph showing the Platteville-Galena carbonate host rock in plane light. (B) Photomicrograph an echinoderm being partially replaced by silica in cross polarized light.

Some of the dolomite rhombs have ferroan rims based on EDS analysis in the SEM. The matrix contains zones of dissolution (figure 19A). Some crystals of dolomite have been completely dissolved with a fibrous rim appearing around the dissolved rhombs, containing some porosity (figure 19A). In other cases, the ferroan dolomite rim is fully dissolved while the center of the dolomites is only partially dissolved (figure 19B). In addition, at least two generations of calcite-filled veins are present within host specimens. Some veins are filled with sparry calcite (figure 20A), whereas other veins contain twinned calcite (figure 20B). Within some host specimens, there are localized zones of brecciation.

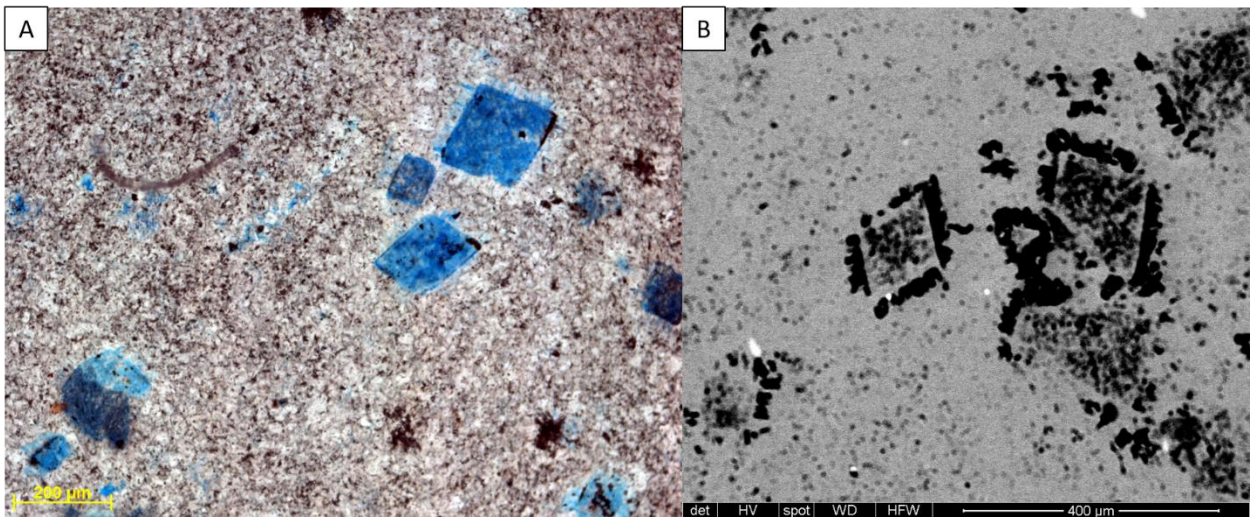

Figure 19: (A) Photomicrograph showing dissolution of the matrix as well as complete dissolution of some dolomite rhombs in plane light. The dissolved rhombs are surrounded by a fibrous rim with some porosity. (B) SEM image of dolomites with dissolution of a ferroan rim and partial dissolution of the rhomb in the center.

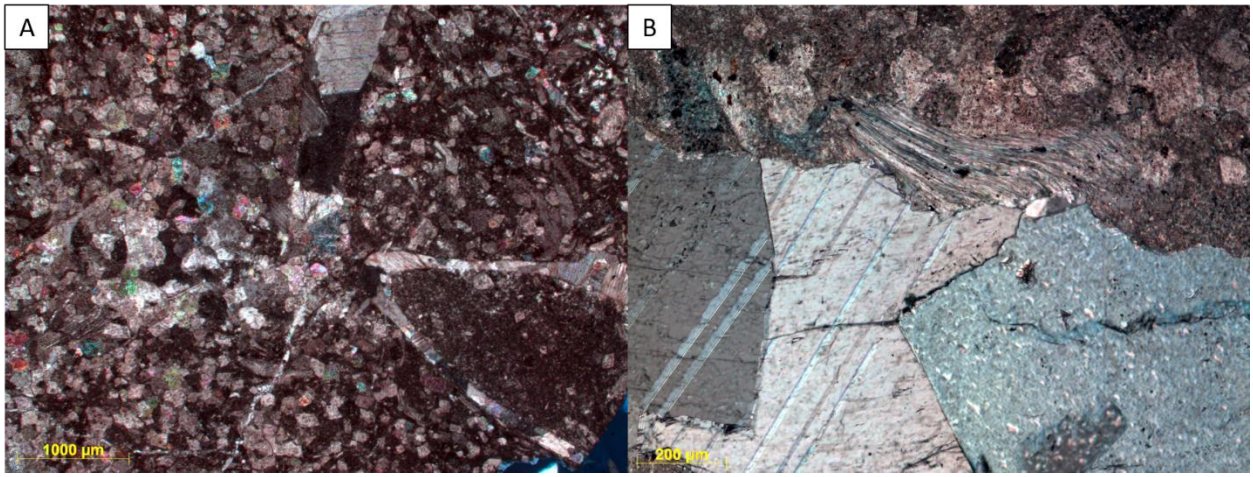

Figure 20: Photomicrographs showing calcite veining in cross polarized light. (A) Sparry calcite veins present within a host specimen, while (B) shows twinning of calcite within a vein.

Diagenesis of the Transition Zones

When the polymict breccia dikes are emplaced, they disrupted the host carbonate near to the injection site. These transition areas are brecciated with numerous veins present. Some veins are filled with secondary sparry calcite and are surrounded by hydrothermal phases such as baroque dolomite (figure 21A&B).

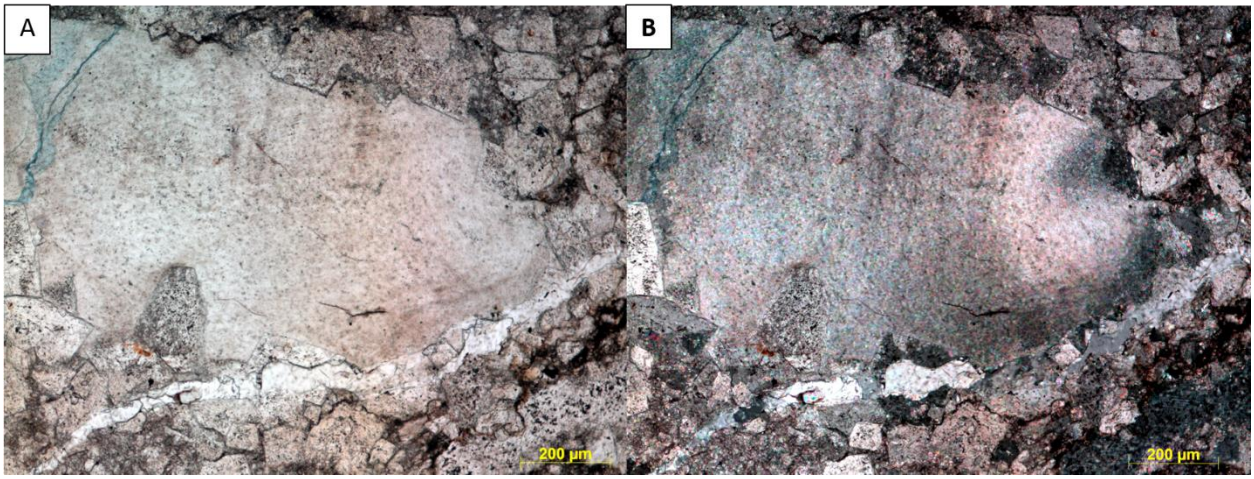

Figure 21: Photomicrograph showing a secondary calcite vein associated with a hydrothermal phase of baroque dolomite within the transition zone in (A) plane light and (B) cross-polarized light.

Brecciated veins are filled with fragments of host carbonate and phases such as clays, pyrite, calcite and dolomite, quartz, gypsum and apatite (figure 22A&B). These veins display an alignment of mineral grains and the phases are interpreted to be part of a suevite like flow (Newsom et al., 1986). The apatite and gypsum have elongated shapes (figure 22A&B) in some flows. The clays, mostly illite based on EDS analysis, dominate the flow with pyrite grains and framboids scattered throughout.

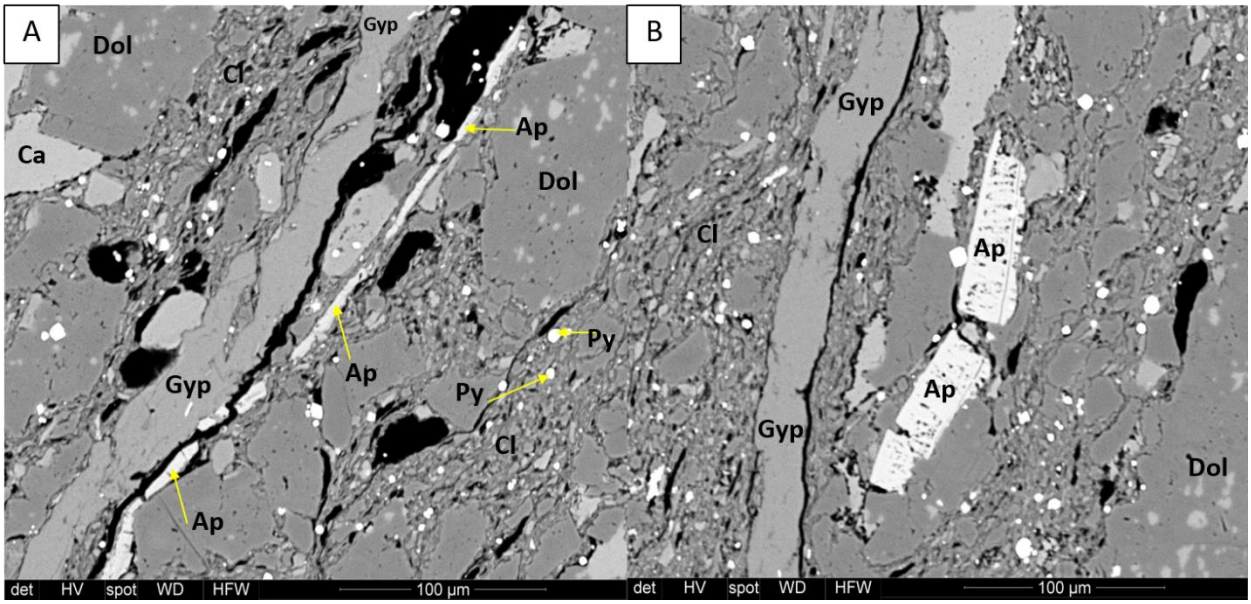

Figure 22: (A) and (B) show SEM backscatter images of the suevite-like flow. Note the alignment of the phases present such as illite clays (Cl), pyrite (Py), apatite (Ap), gypsum (Gyp), dolomite (Dol) and calcite (Ca). The apatite and gypsum occur as elongate bodies within the flow suggesting they are authigenic. Some apatite in (B) appears more tabular in shape.

Some of the pyrite has been replaced by iron oxides, which based on petrographic characteristics and EDS analysis, is interpreted to be magnetite or goethite. Replacement is seen as iron oxide rims around pyrite, where the pyrite is interpreted to have converted to magnetite (figure 23A&C). Framboids (figure 23B) are also being replaced by an iron oxide, which based on EDS spectra, could be goethite due to the presence of an elevated silica peak. The hematite present at transition zones, is concentrated in small veins (figure 23D). In some of these transition areas, grains of iron oxides and apatite occur in zones with suevite-like flow textures (figure 24A&B).

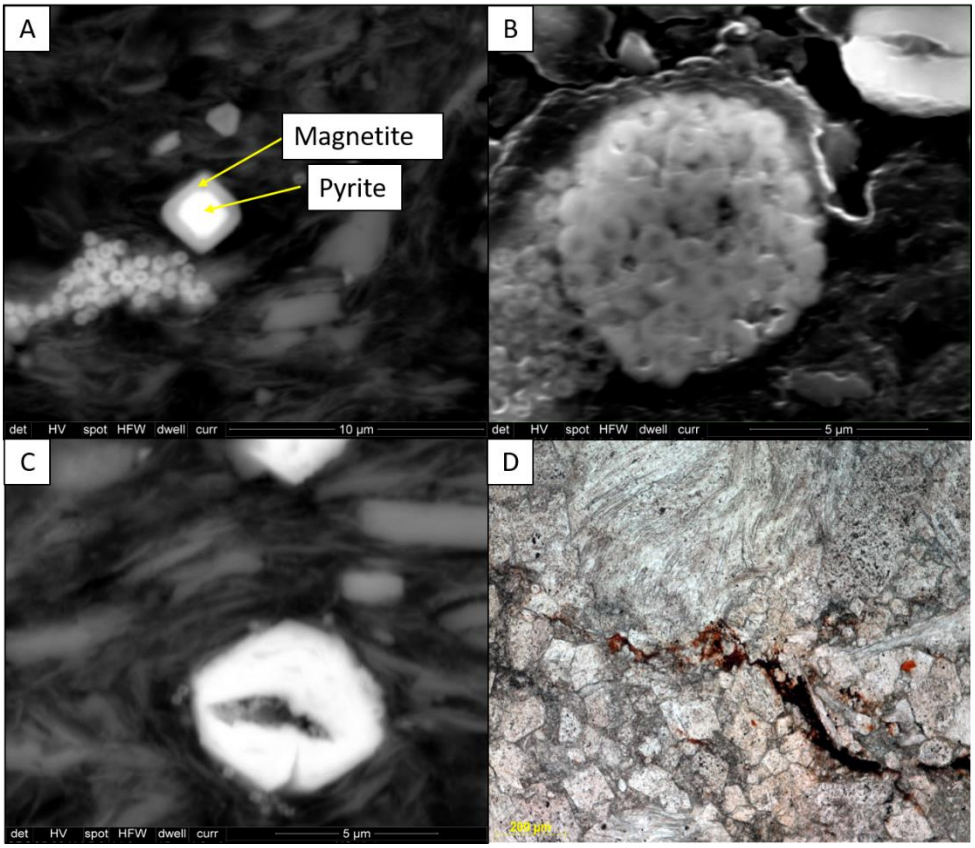

Figure 23: Magnetic phases present in the transition zone. (A) A backscatter SEM image of a pyrite grain being partially replaced by magnetite along with some pyrite framboids being replaced by magnetite. (B) A backscatter SEM image of a pyrite framboid being partially replaced by an iron oxide with a hint a silica, indicating it may be goethite. (C) A backscatter SEM image of an iron oxide surrounded by clays. (D) A thin section showing a small vein filled with hematite in plane light.

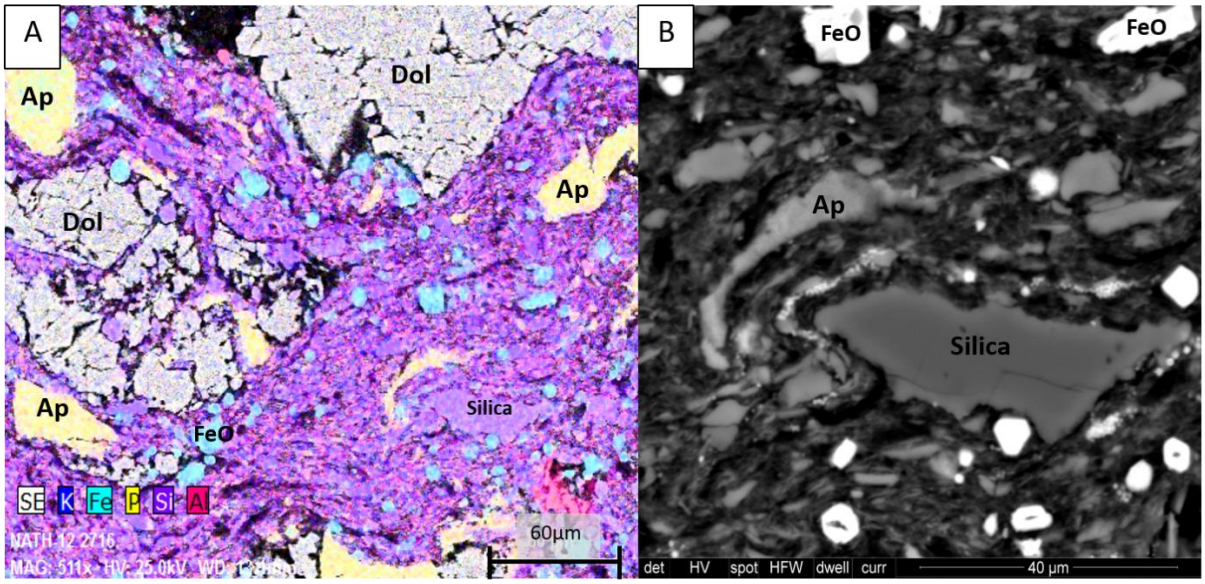

Figure 24: (A) shows an SEM backscatter image co-rendered with an elemental map to highlight different phases. The alignment of minerals again suggests a fluidized suevite-like flow. Phases include apatite (Ap), Silica, iron oxides (FeO) and dolomite (Dol). One dolomite clast appears to have been brecciated in place before the flow, allowing the clays and other phases to move through the clast. (B) Example of authigenic apatite that curves around a silica grain, suggesting precipitation during the flow.

Diagenesis of the Polymict Breccias

The breccias are composed of dolomite crystals, clasts of host carbonate and clasts derived from other lithologies (figure 25A). The dominant constituent is angular and fractured dolomite crystals. Some of these dolomites are zoned with ferroan rims (figure 25B). Vuggy porosity is prevalent in the breccias (figure 25B). Some of the vugs are spheroidal, while some vugs maintain the shape of the dolomite rhombs that once made up the area (figure 25B). Intraparticle porosity also occurs as partially to completely dissolved dolomite crystals. Within certain breccia specimens, some calcite exhibited a feathery texture (Morrow and Weber, 2009 & Jones et al., 2000) (figure 26A). Some of this calcite was also replaced by silica (figure 26B).

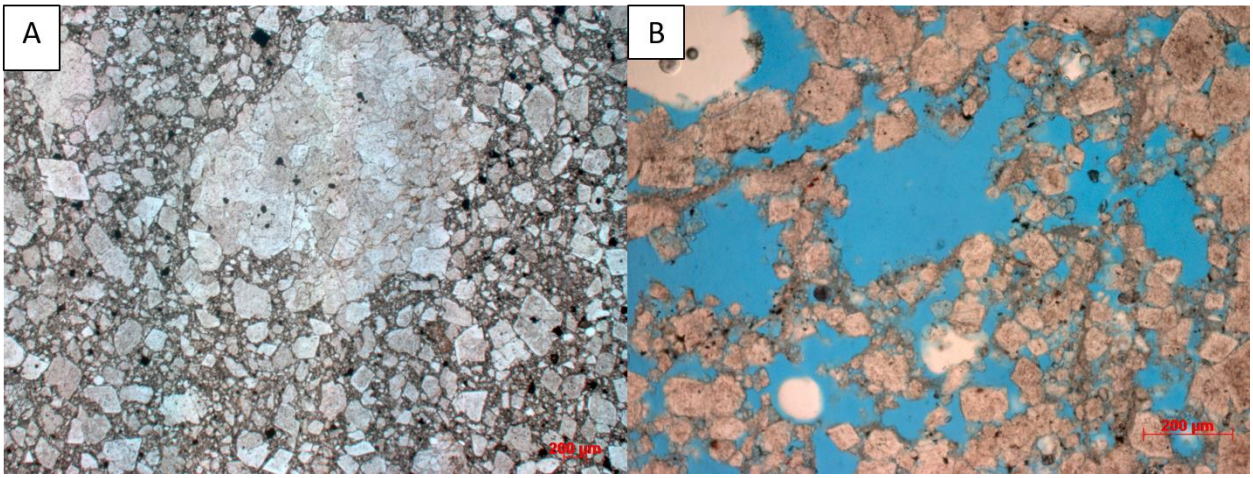

Figure 25: (A) Photomicrographs of the Polymict breccias in plane light. The breccias are composed of dolomite crystals and clasts of the host carbonate rock. (B) displays the pervasive vuggy porosity present in the breccias. Upper vugs in the image are spheroidal, while vugs near the bottom of the image keep the shape of the dolomite rhombs that were once there. Some of the dolomite crystals are zoned and, based on EDS analysis, appear to have ferroan rims.

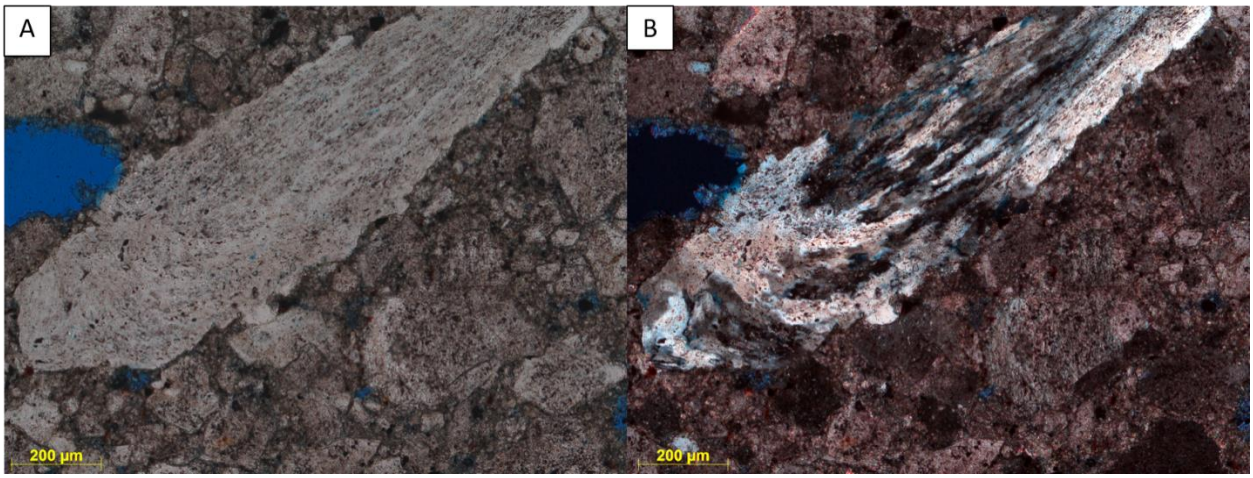

Figure 26: Carbonate material with a wispy texture. (A) Photomicrograph showing the calcite with a wispy texture in plane light. (B) Photomicrograph of the calcite being replaced with silica in cross polarized light.

The breccias also contain clasts of sandstone (figure 27A), sphalerite (figure 27B), quartz grains and rare apatite (figure 27C). Some of the quartz grains contain dust lines and overgrowths, and although some of these overgrowths are euhedral, they were probably inherited from the St. Peter Sandstone located in the quarry. Within some breccias, rare coated grains are present (figure 27D). The coatings contain clays, dolomite, calcite and hexagonal crystals of silica. Based on the euhedral, hexagonal habit of the silica, it could be tridymite (figure 27D).

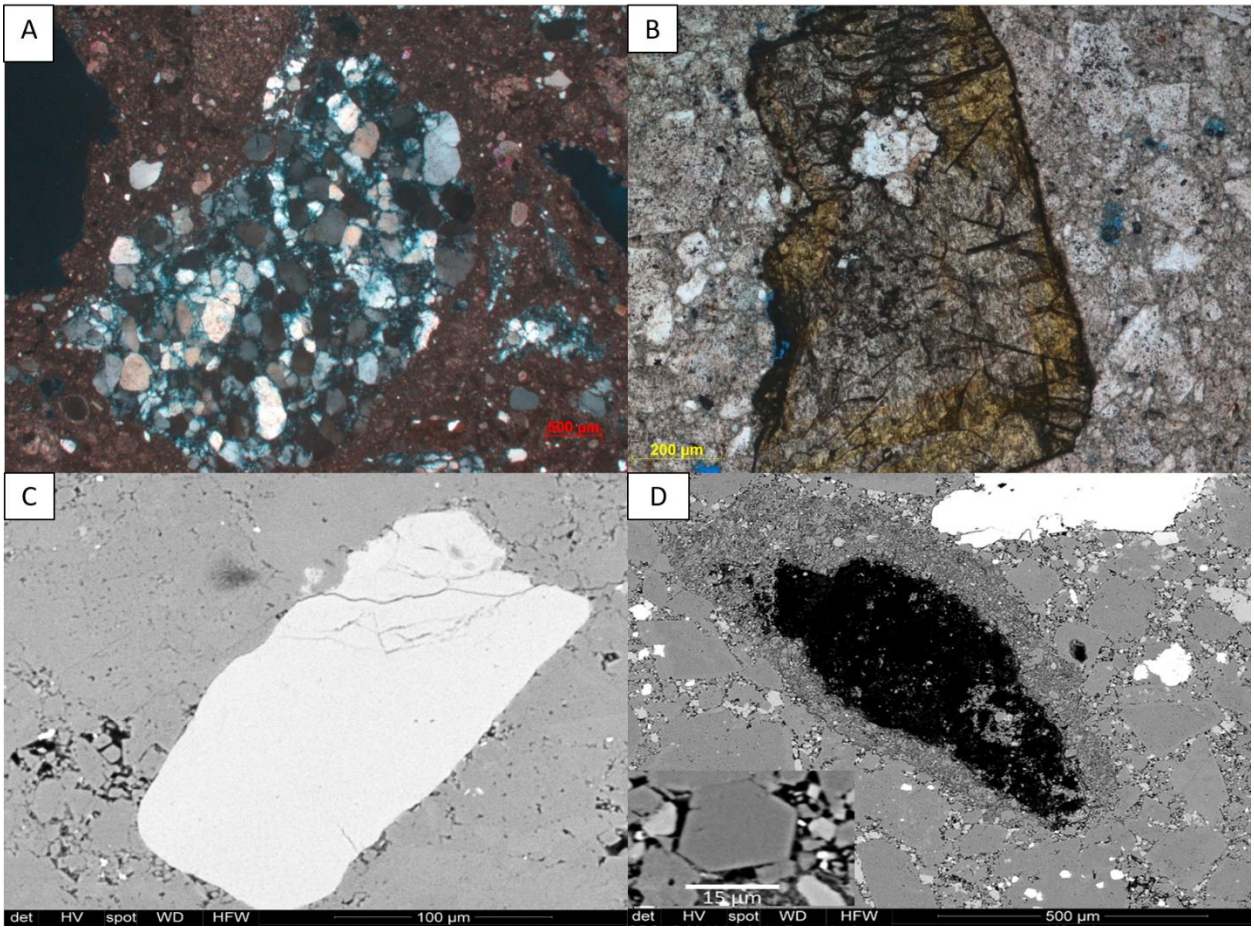

Figure 27: (A) Photomicrograph showing a sandstone clast derived from the St. Peter Sandstone in cross polarized light. There is porosity in between the quartz grains that make up the clast. (B) Photomicrograph showing a sphalerite grain in the polymict breccia in plane light. (C) SEM backscatter image of an apatite grain in the polymict breccia. These gains are detrital and were likely brought in from an external source. (D) SEM backscatter image of a coated grain. The grain itself was plucked during the thin section making process. The coating contains clays, dolomite, calcite and euhedral crystals of silica. The inset image shows the hexagonal habit of the silica. This habit points towards it being Tridymite.

Both magnetite and hematite phases are found in the polymict breccia specimens. These magnetic grains are commonly found replacing other phases. Magnetite occurs via replacement of pyrite grains (figure 28A), while hematite is found replacing gypsum rosettes (figure 28B). Hematite also occurs as a cement between silica grains (figure 28C).

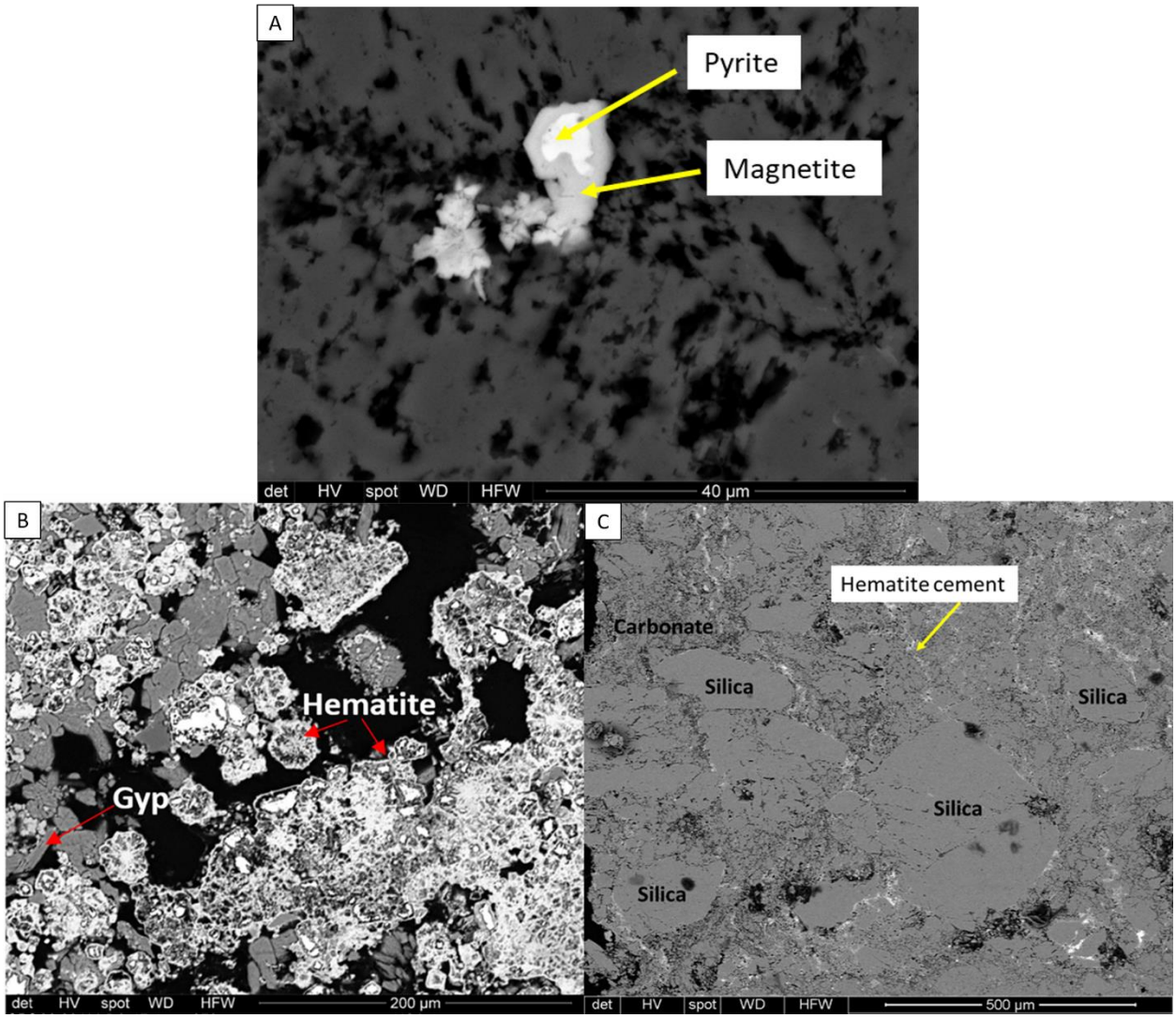

Figure 28: SEM backscatter images of the magnetic phases present in polymict breccia specimens. (A) Pyrite grain being replaced by magnetite. (B) Gypsum rosettes that have been replaced by hematite. (C) hematite occurring as a cement between the silica grains and carbonate groundmass.

Discussion

Origin and Timing of the Magnetization

Demagnetization revealed two distinct components, one with a southerly and up direction and the other with a northerly and down direction. A positive reversal test indicates that the magnetizations were likely obtained during a pole reversal. Results of the tilt test indicate that magnetization was acquired post-tilting, and therefore after the impact occurred. The pole position for the magnetization in the Polymict breccia dikes, as well as the host carbonates at the Kentland impact, indicate a Late Triassic to Early Jurassic timing of remanence acquisition. There were numerous reversed intervals in the Late Triassic – Early Jurassic (for e.g. Muttoni and Kent, 2019, Gallet et al., 2015, Kent and Olsen, 2008 & Steiner, 1980). Dual polarity remagnetizations have been seen in other impact structures (e.g. Carporzen and Gilder, 2006 & Steiner and Shoemaker, 1993).

Analysis of the components show that in dual polarity specimens, the northerly and down direction is most commonly removed at higher temperatures (>450˚C), whereas in single polarity specimens this direction tends to be associated with lower temperatures (≤400˚C). It is likely that this direction is associated with hematite at high temperatures, and magnetite at low temperatures. The southerly and up direction appears to consistently prefer temperatures less than 550˚C, which suggests this direction resides primarily in magnetite.

Rock magnetic experiments, as well as petrographic and SEM analysis, also suggest that the magnetizations reside primarily in magnetite with a minor component residing in hematite. The intermediate temperature component likely resides in magnetite, while the higher temperature component resides in hematite. EDS analysis identified traces of possible goethite; however, it is

not considered to carry a stable remanence. Under certain conditions, goethite can further alter to hematite, so it is possible that the goethite, which altered from pyrite, is a likely source for the hematite which drives the higher temperature component of magnetization (Osinski et al., 2008).

Several possibilities exist for the origin of the ChRMs recorded at Kentland; a shock remanent magnetization (SRM), a thermal remanent magnetization (TRM), a thermoviscous remagnetization (TVRM) or a chemical remanent magnetization (CRM). A post tilting magnetization rules out the possibility of a SRM (Halls, 1979). A thermal remanent magnetization could have been acquired as the dikes were emplaced, due to frictional heating between the dike and host rock contact (Fairchild et al., 2016), however; this would only reset the magnetization in the dike. The surrounding host would remain unchanged. At Kentland we find similar directions in both the host carbonate as well as the polymict breccia dikes, ruling out the possibility of a TRM.

Conodonts in the area have a CAI index of 1.5 indicating temperatures of less than 100˚C (Vatow, 1980). This information combined with maximum unblocking temperatures of 450˚C and 675˚C rules out the possibility of a TVRM in magnetite or hematite (Dunlop et al., 2000, Kent and Miller, 1987 & Kent, 1985)

A CRM, caused by fluids, is a plausible explanation for the origin of the magnetization. The diagenetic analysis provides evidence of hydrothermal phases, such as baroque dolomite, authigenic apatite and gypsum, sylvite and possible tridymite, in the polymict dikes and in some of the host carbonates. Magnetite is interpreted to be replacing pyrite, and authigenic hematite present in some specimens are also consistent with hydrothermal fluids and the subsequent acquisition of a CRM. This along with the suevite-like textures, point toward the passage of hydrothermal fluids within the crater which could have caused acquisition of the CRM.

Jackson and Van Der Voo (1986) proposed a Cretaceous age for the impact, with a single direction of magnetization (northwesterly declinations and steep down inclinations) and low maximum unblocking temperatures of 300˚C- 330˚C. This current study found two antipodal directions of magnetization with much shallower inclinations, which suggests an older, Late Triassic to Early Jurassic age for the impact. Furthermore, the Cretaceous period is marked by a prolonged period of normal polarity, so the reversed component found in this study provides evidence against a mid to late Cretaceous age for the crater. It is possible that the magnetization reported by Jackson and Van der Voo was contaminated by a modern overprint which could have steepened the inclination.

Weber et al. (2005) used detrital apatite found in the St. Peter's Sandstone at Kentland, as well as multiple outcrop and core locations away from the quarry to conduct an apatite fission track study. The apatite grains in the quarry cooled through 135 ˚C at 184 ± 13 Ma in the Jurassic (Weber et al., 2005). This age is slightly younger than the age of the impact and they interpreted this age to date a regional exhumation event rather than the impact event.

Diagenesis of the Impact Crater

Many terrestrial craters around the world contain evidence of hydrothermal alteration. In complex craters, up to 20km in diameter, the temperature increase experienced by the target rocks can be about 100˚C to 120˚C (Osinski et al., 2012). In Kentland, conodonts in the host carbonates have a CAI index of 1.5, which points towards temperatures of approximately 100 ˚C (Votaw, 1980). Allen et al (1982) looked at 12 impact terrestrial impact craters, including the Ries impact crater in Germany which is associated with carbonate rocks. Most of the craters had an assemblage of clay, silica, potassium feldspar and zeolites associated with them, which indicated low pressures (1GPa-5GPa) and temperatures (100°C - 300°C) (Allen et al., 1982). Craters such as the Ries, Manicouagan and Sudbury record assemblages of clay minerals, chlorite, silica, mixed layer illite-chlorite and other minerals that formed between 100°C and 300°C (Pirajno, 2009). These assemblages are consistent with what is seen in both the host and breccia samples from the Kentland impact crater. Furthermore, alteration of impact glass and silicates leads to the production of hydrated phases such as phyllosilicates (Osinski et al., 2012). Clays, such as illite and some smectite, are observed within veins in the host and the polymict breccia dikes at Kentland. Within the dikes, clays are also observed in some vugs and between grains. According to Allen et al., (1982) it is common to find clays in impact breccias. Within the host carbonates, two generations of veining are observed. There are calcite veins that exhibit twining, which formed prior to the impact. There are also sparry calcite veins without twining that were formed post-impact and are interpreted to be related to fluid movement and reprecipitation of calcite soon after the impact occurred.

Hydrothermal systems also result in the remobilization and deposition of sulfides in breccias and fracture zones (Pirajno, 2009). In both the host and breccia in the Kentland impact,

there is pyrite as well as rare detrital galena present. The pyrite seems to be concentrated within the clay rich flows, although it is seen throughout the host and breccia. Pyrite framboids may represent early diagenesis while pyrite cubes may represent a later phase of activity. Authigenic gypsum found within veins at Kentland, is a common late hydrothermal product produced in impacts and represents the remobilization of sulfates within the carbonate rocks (Osinski et al., 2012). Authigenic apatite is also seen in the suevite-like flows and provides evidence for hydrothermal fluids. These suevite-like flows are similar to what has been found in the Ries (Newsom et al., 1986) and Chicxulub (Wittmann et al, 2004) impact craters. Goethite is found replacing pyrite framboids (figure 23B) and it is a common alteration product from iron sulfide weathering. Goethite can also further alter to hematite under certain conditions, creating a likely source for the hematite seen within the specimens (Osinski et al.,2012).

Rare coated grains seen within the breccia are likely formed via a process similar to the formation of volcanic accretionary lapilli (e.g., Gilbert and Lane, 1994). The accretion of fine fragments and minerals around rock fragments or liquid can occur during the excavation stage of the crater, and is described in the Ries crater (Graup, 1981) and in the Chicxulub crater (Sagla et al., 2000 & Jones et. al, 2000). They have been reported in polymict breccia dikes at the Azuara and Rubielos de la Cérida impact in Spain (Ernston & Claudin, 2019). The coated grains within the Kentland crater contain possible tridymite, which is a high temperature polymorph of quartz. Tridymite also contributes to the hydrothermal phases present at Kentland. Research is ongoing to confirm that the hexagonal silica is in fact tridymite.

The dissolution of the matrix as well as vugs present in both the host rock and the polymict breccia dikes are believed to be due to devolatilization of the carbonate rock, probably related to the expulsion of water vapor and CO_2 from the carbonate rich impact zone, as well as the passage

of hydrothermal fluids throughout the impact (Bjørnerud, 1997). Osinski et al., (2008) mention that sedimentary rocks are especially rich in volatiles such as CO_2 and H_2O due to carbonates as well as water present in hydrous minerals. Decarbonation of limestone or dolomite produces a free volatile phase and calcite breaks down to CaO and CO2 at about 450kbar (Kieff and Simmons, 1980). Pure Carbonates can form highly reactive oxides which can recombine into carbonates during the excavation stage in an impact. Surface exposed limestone would be more likely to decarbonate, and decarbonation under low shock pressures and temperatures would likely take place during post shock cooling (Jones et al., 2000). It is likely that a decarbonation event took place during the formation of the Kentland crater. Another key feature that provides evidence for some sort of decarbonation are the feathery textures (Morrow and Weber, 2009) that are seen in the host carbonate rock in the Kentland impact crater. Carbonates with feathery textures (figure 26A&B) at the Chicxulub impact crater are attributed to quenched carbonate melts (Jones et al., 2000, Osinski et al, 2013). These carbonates make up about 10% of the breccias at Chicxulub. Pirajno (2009) also reported finding bladed calcite in some impacts which is indicative of boiling CO2 bearing fluids. These bladed calcites are sometime replaced by quartz (figure 26B) (Pirajno, 2009).

Euhedral clasts of apatite and sphalerite occur in the polymict breccias (figure 27B&C). The sphalerite is believed to have been ripped up from a sulfide mineralization event that occurred between the Pennsylvanian and the Permian (Bjørnerud, 1997). The source of iron in the pyrite may have come from dissolved Fe-rich dolomite and the MVT type deposits may provide a source of sulphur. The sylvite crystals that formed in some of the porosity within the host rock may be due to cooling saline brines that may have been flowing through the crater (Rubin et al., 2002). The fluids moving throughout the crater may have been evaporated, resulting in a more saline

brine in the late stages of crater formation (Rubin et al., 2002). Sylvite usually precipitates at temperatures <100°C.

The features at Kentland are common in many other impact structures, regardless of lithology. Pirajno (2005) describes a model for hydrothermal processes at work in terrestrial impact craters. This model involves two main stages. In the first stage, melt sheets provide the heat to allow hydrothermal fluids to circulate (Pirajno, 2005). This stage is associated with temperatures of 500°C - 600°C (Pirajno, 2005). At Kentland, there is a lack of evidence for the melt sheet, however this crater was eroded and furthermore, there tends to be a lack of obvious melt products in decarbonated limestones (Kieff and Simmons, 1980). Furthermore, carbonate melt may be hard to distinguish with petrographic and SEM analysis alone. Microprobe analysis can aid in distinguishing melts. Osinski et al., (2005) report higher weight percentages of MgO, Al_2O_3, SiO_2 and FeO in calcite filling impact breccias at the Haughton impact, than the calcite developed in the carbonate host rocks. Further work utilizing microprobe analysis may help characterize some of the melt phases present in the Kentland crater.

According to Pirajno (2005) the second hydrothermal stage is characterized by temperatures of 500°C and by fracture controlled hydrothermal fluids (Pirajno, 2005). Hot rock in the central uplift provides heat, and as such this area is the most affected (Pirajno, 2005). The hot fluids move along the crater walls and in fractures in the rocks to produce hydrothermal minerals such as clays, calcite, hematite and quartz (Pirajno, 2005). At Kentland, the suevite-like flows which exist in the transition zone between the host and the breccias, may be explained by these fracture controlled hydrothermal fluids, as they are dominated by clays, calcite and quartz. The boiling of CO2 rich fluids may also cause bladed calcite to form in this stage (Pirajno, 2005).

Clasts found in the breccia dikes were stratigraphically separated from their original lithology by 100s of meters (Laney and Van Schmus, 1978) and the transport of materials over those distances requires a highly energetic process (Stöffler, 1977). The emplacement of the dikes probably take place during crater growth when material moves up the walls with a high particle motion (Stöffler, 1977). Breccias in the Kentland impact were also interpreted to have been emplaced as a suspension in the CO_2 rich water that may have moved through the system as a result of the decarbonation (Laney and Van Schmus, 1978).

Many of the mineral phases identified within the crater point towards the passage of hydrothermal fluids. This combined with the suevite-like flows point towards the passage of hydrothermal fluids. The CRM is found in the breccias and host carbonates with the minerals indicating alteration by hydrothermal fluids, and it is these fluids that are interpreted to have caused acquisition of the Late Triassic to Early Jurassic CRM. These fluids likely aided in the emplacement of the breccias and continued for some time after the impact occurred, Due to this, the age of the CRM is the maximum possible age of the impact although it probably dates the impact since the fluids occurred soon after the impact.

Conclusion

Paleomagnetic, rock magnetic, petrographic and SEM analysis of the polymict breccia dikes and the host carbonate rocks at the Kentland impact crater, provide improved constraints on the age of the crater as well as provide new insights into diagenetic changes that have occurred since the occurrence of the impact. The key conclusions are:

1. The Kentland impact crater has a post tilting late Triassic – early Jurassic chemical remanent magnetization. This magnetization has two components; an intermediate temperature component residing in magnetite, and a higher temperature component residing in hematite. These components have antipodal directions and are interpreted to have been acquired during a pole reversal. The source of the CRM is likely the passage of post impact hydrothermal fluids within the crater. The CRM is the maximum possible age of the crater and probably dates the impact since the hydrothermal fluids altered the rock soon after the impact occurred.
2. The source of the CRM is likely the passage of post impact hydrothermal fluids within the crater. Petrographic and SEM analysis reveal evidence of hydrothermal mineral phases such as baroque dolomite, authigenic gypsum and apatite, magnetite, sylvite and possible tridymite. These phases are concentrated within possible suevite flows dominated by illite clays in the host rock. At least two generations of calcite veining occur, which point toward post impact late infill of voids as well as preimpact early calcite fill.
3. Impact generated melt may exist at the Kentland impact perhaps as recrystallized carbonate material and as suevite-like flows within veins. The pervasive vuggy porosity within the breccias provide evidence of devolatilization of CO_2 and CO_2

degassing, and calcite with feathery textures points toward quenching of melt. Further microprobe analysis is needed to quantify the weight percentages of certain oxides with carbonate matrix to determine evidence of carbonate melt.

References

Alder, A., Weber, J., Laó-Dávila, D. & Pope, M., 2017. Geological mapping, fault-slip and GigapanTM image analysis, Kentland impact structure, Indiana, USA [abs.]. *Geological Society of America Abstracts with Programs,* 49(2).

Allen, C. C., Gooding, J. L. & Keil, K., 1982. Hydrothermally altered impact melt rock and breccia: Contributions to the soil of Mars. *Journal of Geophysical Research: Solid Earth,* 87(B12), pp. 10083-10101.

Bjørnerud, M. G., 1998. Superimposed deformation in seconds: breccias from the impact structure at Kentland, Indiana (USA). *Tectonophysics,,* 290(3-4), pp. 259-269.

Bottomley, R. J., York, D. & Grieve, R. A. F., 1978. 40 Ar-39 Ar ages of scandinavian impact structures: I Mien and Siljan. *Contributions to Mineralogy and Petrology,* 68(1), pp. 79-84.

Carporzen, L. & Gilder, S. A., 2006. Evidence for coeval Late Triassic terrestrial impacts from the Rochechouart (France) meteorite crater. *Geophysical Research Letters,* 33(19).

Chamberlin, R. T., 1923. On the crustal shortening of the Colorado Rockies. *American Journal of Science,* Issue 33, pp. 215-221.

Cisowski, S. M. & Fuller, M., 1978. The effect of shock on the magnetism of terrestrial rocks. *Journal of Geophysical Research: Solid Earth,* 83(B7), pp. 3441-3458.

Cohen, A. J., Reid, A. & Bunch, T. E., 1962. Central uplifts of terrestrial and lunar craters, (Part 1) Kentland and Serpent Mound structures. *Journal of Geophysical Research,* 76(4), pp. 1632-1633.

Collett, J., 1883. *Geological Survey of Newton County. Indianapolis:,* s.l.: B. Burford, State Contractor for Printing and Binding.

Collinson, C., Sargent, M. L., Jennings, J. R. & Sloss, L. L., 1988. *Illinois basin region. Sedimentary cover—North American craton, US.* Boulder Colorado: Geological Society of America, Geology of North America.

Cummings, E. R. & Shrock, R. R., 1928. *The geology of the Silurian rocks of northern Indiana (No. 75),* s.l.: WB Burford Print Company..

Dietz, R. S., 1947. Meteorite impact suggested by the orientation of shattercones at the Kentland, Indiana disturbance. *Science,* Volume 105, p. 47.

Dietz, R. S., 1960. Meteorite impact suggested by shatter cones in rock. *Science,* Volume 131, pp. 1781-1784.

Dunlop, D. J. & Argyle, K. S., 1991. Separating multidomain and single-domain-like remanences in pseudo-single-domain magnetites (215–540 nm) by low-temperature demagnetization. *Journal of Geophysical Research,* 96(B2), pp. 2007-2017.

Dunlop, D. J., O¨ . O¨ zdemir, Clark, D. A. & Schmidt, P. W., 2000. Time-temperature relations for the remagnetization of pyrrhotite (Fe7S8) and their use in estimating paleotemperatures. *Earth Planetary Science Letters,* Volume 176, pp. 107-116.

Egli , R., 2003. Analysis of the field dependence of remanent magnetization curves. *Journal of Geophysical Research: Solid Earth,* 108(B2).

Elmore, R. D. & Dulin, S., 2007. New paleomagnetic age constraints on the Decaturville impact structure and Weaubleau structure along the 38th parallel in Missouri (North America). *Geophysical research letters,* 34(13).

Ernston, K. & Claudin, F., n.d. *Ernston Claudin Impact Strructures - Meterorite Craters.* [Online]
Available at: http://www.impact-structures.com/impact-spain/the-rubielos-de-la-cerida-impact-basin/accretionary-lapilli-in-the-suevitic-basal-breccia/
[Accessed 18 April 2019].

Fairchild, L. M., Swanson-Hysell, N. L. & Tikoo, S. M., 2016. A matter of minutes: Breccia dike paleomagnetism provides evidence for rapid crater modification. *Geology,* 44(9), pp. 723-726.

Fisher, R. A., 1953. Dispersion on a sphere. *Proceedings of the Royal Society of London. Series A. Mathematical and Physical Sciences,* 217(1130), pp. 295-305.

French, B. M., 1998. Traces of Catastrophe: A Handbook of Shock-Metamorphic Effects in Terrestrial Meteorite. *LPI Contribution No. 954, Lunar and Planetary Institute, Houston,* p. 120 .

Gallet, Y., Pavlov, V., Shatsillo, A. & Hulot, G., 2015. Constraining the reversing and non-reversing modes of the geodynamo. New insights from magnetostratigraphy. In: *AGU Fall Meeting Abstracts.* s.l.:s.n.

Gilbert, J. S. & Lane, S. J., 1994. The origin of accretionary lapilli.. *Bulletin of Volcanology,* 56(5), pp. 398-411.

Gorby, S. S., 1886. *The Wabash Arch,* s.l.: William B. Burford, Contractor for State Printing and Binding.L. C.

Graup, G., 1981. Terrestrial chondrules, glass spherules and accretionary lapilli from the suevite, Ries Crater, Germany. *Earth and Planetary Science Letters,* Volume 55, pp. 407-418.

Grieve, R. A. F., Robertson, P. B. & Dence, M. R., 1981. *Constraints on the formation of ring impact structures, based on terrestrial data In: Multi-ring basins: Formation and evolution; Proceedings of the Lunar and Planetary Science Conference.* Houston, TX, November 10-12, New York and Oxford, Pergamon Press, 1981, p. 37-57, pp. 37-57.

Grieve, R. A. & Pesonen, L. J., 1996. Terrestrial impact craters: their spatial and temporal distribution and impacting bodies. In: *In Worlds in Interaction: Small Bodies and Planets of the Solar System.* Dordrecht: Springer, pp. 357-376.

Grieve, R. A. & Pilkinton, M., 1996. The signature of terrestrial impacts. *AGSO Journal of Australian Geology and Geophysics,* 16(4), pp. 399-420.

Gutschick, R. C., 1972. *Geology of the Kentland Structural Anomaly, Northwestern Indiana: Field Guide for the 35th Annual Meeting of the Meteoritical Society.* Chicago, s.n.

Gutschick, R. C., 1983. Geology of the Kentland Dome structurally complex anomaly, northwestern Indiana (Field Trip 5). In: R. H. Shaver & J. A. Sunderman, eds. *Field Trips in Midwestern Geology: Bloomington, Indiana, Geological Society of America, Indiana Geological Survey, and Indiana University Department of Geology, Guidebook.* s.l.:s.n., pp. Vol. 1, 105-138.

Gutschick, R. C., 1987. The Kentland Dome, Indiana: A structural anomaly. In: D. L. Biggs, ed. *North-Central Section of the Geological Society of America Centennial Field Guide.* Boulder, Colorado: s.n., pp. Vol. 3, 337-342.

Halls, H. C., 1979. The Slate Islands meteorite impact site: A study of shock remanent magnetization. *Geophysical Journal International,* 59(3), pp. 553-591.

Jackson, M. & Van Der Voo, R., 1986. A paleomagnetic estimate of the age and thermal history of the Kentland, Indiana cryptoexplosion structure. *The Journal of Geology,* 94(5), pp. 713-723.

Jones, A. P., Claeys, P. & Heuschkel, S., 2000. Impact melting of carbonates from the Chicxulub crater. In: Heidelberg, ed. *Impacts and the early Earth.* Berlin: Springer, pp. 343-361.

Jourdan, F., Reimold, W. U. & Deutsch, A., 2012. Dating terrestrial impact structures. *Elements,* 8(1), pp. 49-53.

Kenkmann, T. & Dalwigk, I., 2000. Radial transpression ridges: A new structural feature of complex impact craters. *Meteoritics & Planetary Science,* 35(6), pp. 1189-1201.

Kent, D. V., 1985. Thermoviscous remagnetization in some Appalachian limestones. *Geophysical Research Letters,* Volume 12, pp. 805-808.

Kent, D. V. & Miller, J. D., 1987. Redbeds and thermoviscous magnetization theory. *Geophysical Research Letters,* 14(4), pp. 327-330.

Kent, D. V. & Olsen, P. E., 2008. Early Jurassic magnetostratigraphy and paleolatitudes from the Hartford continental rift basin (eastern North America): Testing for polarity bias and abrupt polar wander in association with the central Atlantic magmatic province. *Journal of Geophysical Research: Solid Earth,* 113(B6).

Kieffer, S. W. & Simonds, C. H., 1980. The role of volatiles and lithology in the impact cratering process. *Reviews of Geophysics,* 18(1), pp. 143-181.

Kirschvink, J. L., 1980. The least-squares line and plane and the analysis of palaeomagnetic data. *Geophysical Journal International,* 62(3), pp. 699-718.

Koeberl, C. & Anderson, R. R., 1996. *The Manson Impact Structure, Iowa; Anatomy of an Impact Crater (Vol 302).* s.l.:Geological Society of America.

Koeberl, C. & Sharpton, V., 1993. Geochemical study of rocks from the Kentland, Indiana, impact structure; progress report. *Meteoritics*, 28(3), p. 382.

Kolata, D. R. & Nelson, W. J., 1990. *Tectonic History of the Illinois Basin: Chapter 18: Part I. Illinois Basin: Evolution.*. s.l.:s.n.

Kontny, A. et al., 2007. Petrography and shock-related remagnetization of pyrrhotite in drill cores from the Bosumtwi Impact Crater Drilling Project, Ghana. *Meteoritics & Planetary Science*, 42(4-5), pp. 811-827.

Kruiver, P. P., Dekkers, M. J. & Heslop, D., 2001. Quantification of magnetic coercivity components by the analysis of acquisition curves of isothermal remanent magnetisation. *Earth and Planetary Science Letters,* 189(3-4), pp. 269-276.

Laney, R. T. & Van Schmus, W. R., 1978. *A structural study of the Kentland, Indiana impact site: A structural study of Kentland, Indiana, impact site: Proceedings of the Ninth Lunar and Planetary Science Conference.* Houston, Texas, The Moon and the inner solar system: New York, Pergamon Press, p. 2609–2632.

Lowrie, W., 1990. Identification of ferromagnetic minerals in a rock by coercivity and unblocking temperature properties. *Geophysical Research Letters,* Volume 17, pp. 159-162.

McElhinny, M. W., 1964. Statistical significance of the fold test in palaeomagnetism. *Geophysical Journal International,* 8(3), pp. 338-340.

McFadden, P. L. & Lowes, F. J., 1981. The discrimination of mean directions drawn from Fisher distributions. *Geophysical Journal International,* 67(1), pp. 19-33.

Melosh, H. J. & Ivanov, B. A., 1999. Impact crater collapse. *Annual Review of Earth and Planetary Sciences,* Volume 27, pp. 385-415.

Morrow, J. & Weber, J., 2009. *Comparison of low-pressure shock-metamorphic effects in quartz from the Barringer crater, Arizona and the Kentland dome, Indiana [abs.]: 40th Lunar and Planetary Science Conference.* Woodlands, Texas, LPI Contribution No. 1468, 1913.pdf.

Muttoni, G. & Kent, D. V., 2019. Jurassic monster polar shift confirmed by sequential paleopoles from Adria, promontory of Africa. *Journal of Geophysical Research: Solid Earth.*

Newsom, H. E., Graup, G., Sewards, T. & Keil, K., 1986. Fluidization and hydrothermal alteration of the suevite deposit at the Ries crater, West Germany, and implications for Mars.. *Journal of Geophysical Research: Solid Earth,* 91(B13), pp. E239-E251.

Osinski, G. R. & Pierazzo, E., 2013. *Impact cratering: Processes and products.* Hoboken, New Jersey: John Wiley & Sons.

Osinski, G. R., Spray, J. G. & Grieve, R. A. F., 2008. Impact melting in sedimentary target rocks: An assessment. *SPECIAL PAPERS-GEOLOGICAL SOCIETY OF AMERICA,* Volume 437, p. 1.

Osinski, G. R., Spray, J. G. & Lee, P., 2005. Impactites of the Haughton impact structure, Devon island, Canadian high Arctic. *Meteoritics & Planetary Science,* 40(12), pp. 1789-1812.

Osinski, G. R. et al., 2013. Impact-generated hydrothermal systems on Earth and Mars. *Icarus,* 224(2), pp. 347-363.

Pesonen, L. J., Marcos, N. & Pipping, F., 1992. Palaeomagnetism of the Lappajärvi impact structure, western Finland. *Tectonophysics,,* 216(1-2), pp. 123-142.

Pilkington, M. & Grieve, R. A. F., 1992. The geophysical signature of terrestrial impact craters. *Reviews of Geophysics,* 30(2), pp. 161-181.

Pirajno, F., 2005. Hydrothermal processes associated with meteorite impact structures: evidence from three Australian examples and implications for economic resources. *Australian Journal of Earth Sciences,* 52((4-5)), pp. 587-605.

Pirajno, F., 2009. Hydrothermal processes associated with meteorite impacts. In: *Hydrothermal processes and mineral systems.* Dordrecht: Springer, pp. 1097-1130.

Reynolds, R. L., Goldheber, M. B. & Snee, L. W., 1997. *Paleomagnetic and 40Ar/39Ar Results from the Grant Intrusive Breccia and Comparison to the Permian Downeys Bluff Sill--evidence for Permian Igneous Activity at Hicks Dome, Southern Illinois Basin (No. 2094).* s.l.:US Government Printing Office.

Robertson, D. J. & France, D. E., 1994. Discrimination of remanence-carrying minerals in mixtures, using isothermal remanent magnetisation acquisition curves. *Physics of the Earth and Planetary interiors,* 82(3-4), pp. 223-234.

Rubin, A. E., Zolensky, M. E. & Bodnar, R. J., 2002. The halite-bearing Zag and Monahans (1998) meteorite breccias: Shock metamorphism, thermal metamorphism and aqueous alteration on the H-chondrite parent body. *Meteoritics & Planetary Science,* 37(1), pp. 125-141.

Sagle, T., Tagle, R. & Claeys, P., 2000. Accretionary lapilli from the K–T boundary site of Guayal, Mexico: preliminary insights of expansion plume formation. *63th Annual Meeting, Meteoritical Society,* Volume 5124.

Sloss, L., 1963. Sequences in the cratonic interior of North America. *Bulletin of the Geological Society of America,* 74(2), pp. 93-114.

Steiner, M. B., 1980. Investigation of the geomagnetic field polarity during the Jurassic. *Journal of Geophysical Research: Solid Earth,* 85(B7), pp. 3572-3586.

Steiner, M. B. & Shoemaker, E. M., 1993. Two-polarity magnetization in the Manson impact breccia. *Lunar and Planetary Science Conference,* Volume 24.

Stöffler, D., 1977. Research drilling Nördlingen 1973: Polymict breccias, crater basement, and cratering model of the Ries impact structure. *Geologica Bavarica,* Volume 75, pp. 443-458.

Torsvik,, T. H. et al., 2012. Phanerozoic polar wander, palaeogeography and dynamics. *Earth-Science Reviews,* 114(3-4), pp. 325-368.

Urrutia-Fucugauchi, J., Soler-Arechalde, A. M., Rebolledo-Vieyra, M. & Vera-Sanchez, P., 2004. Paleomagnetic and rock magnetic study of the Yaxcopoil-1 impact breccia sequence, Chicxulub impact crater (Mexico). *Meteoritics & Planetary Science,* 39(6), pp. 843-856.

Votaw, R. B., 1980. Middle Ordovician conodonts from the Kentland structure. *Geological Society of America Abstracts with Program,* Volume 12, p. 259.

Ward, L. C., 1906. *Roads and road materials of the northern third of Indiana,* s.l.: Ind. Dept. Geol. and Nat. Res., 30th Ann. Rept, p.216..

Weber, J. C. et al., 2018. On the backs of giants: Geology of the Kentland impact structure, Newton County (Kentland) Quarry, Indiana (USA)—Building on Ray Gutschick's legacy.. *Ancient Oceans, Orogenic Uplifts, and Glacial Ice: Geologic Crossroads in America's Heartland,* Volume 51, p. 393.

Weber, J. C. et al., 2005. The Kentland impact crater, Indiana (USA): An apatite fission-track age determination attempt. In: *Impact tectonics.* Berlin, Heidelberg: Springer, pp. 447-466.

Wittmann, A. et al., 2004. Impact-related dike breccia lithologies in the ICDP drill core Yaxcopoil-1, Chicxulub impact structure, Mexico. *Meteoritics & Planetary Science,* 39(6), pp. 931-954.